



Afshin Anssari-Benam 

A generalised $W(I_1, I_2)$ strain energy function of binomial form with unified applicability across various isotropic incompressible soft solids

Received: 13 May 2023 / Revised: 20 July 2023 / Accepted: 26 July 2023 / Published online: 1 September 2023
© The Author(s) 2023

Abstract A generalised $W(I_1, I_2)$ strain energy function, a generalisation of previously devised response functions W_1 and W_2 , of binomial form is presented in this work for application to the finite deformation of isotropic incompressible soft solids. It is shown that the proposed model is the *parent* to many of the well-known existing invariants-based models in the literature. The first-order expansion of the model, with six model parameters, is then applied to extant multiaxial deformation of a wide range of materials, from filled and unfilled rubbers to hydrogels, liquid crystal elastomers and biomaterials. The model captures the experimental data accurately, with typical relative errors below 4%, while favourably modelling various challenging mechanical behaviours such as the asymmetry of compression—tension, high nonlinearity of the simple shear response, deformation softening effects, pronounced Payne effect, the *soft elasticity* phenomenon, and the *reverse* Poynting effect. The *predictive* capabilities of the model are also demonstrated and verified against experimental data. Given the analyses and results presented here, the devised model is proposed to serve as a standard choice for a priori selection for application to the finite deformation of isotropic incompressible soft materials.

1 Introduction

Since the introduction of the classical neo-Hookean model by Treloar [1] in 1943 and the enhanced model of Mooney [2] and its generalised form by Rivlin [3] in 1948, numerous developments have been made to the basic theory and several constitutive models have been presented. The assortment of the existing hyperelastic strain energy functions W in the literature, in addition to undermining the notion of *universality* of those models as discussed by Destradre et al. [4], has made the *a priori* selection of a reliable model by engineers and end users a formidable challenge.¹ The most recently published reviews of the state-of-the-art, e.g. [5] in 2023, still echo the observations of Marckmann and Verron [6] in 2006, as well as those conducted and published in between (e.g. [7–11] *inter alia*), that: (i) most models which capture the deformation of a certain class of soft solids (say, unfilled rubbers) struggle with satisfactorily capturing the deformation behaviour of another type(s), say filled rubbers; (ii) many models do not provide as good a fit to the multiaxial deformation datasets of the same specimen with a single set of model parameter values; and (iii) most models do not provide a good *prediction* of the behaviour of specimens if calibrated with data from other deformations. Depending on the emphasis and the angle of approach, each of the cited reviews also confer additional specific shortcomings;

¹ Selection of a *reliable model* for *engineering* applications from the existing choice of models in the literature has been identified as a *challenge* in nearly all of the review articles known to the author, almost word by word, some of which will be cited in the sequel.

however, the foregoing three traits are a common conclusion in all of such studies. These results, shared between microstructural-based and phenomenological models alike, indicate that a standard² model, much less a universal one, for a confident all-purpose generic application to the finite deformation of various soft solids is still lacking in the literature.

The author's own recent endeavours [12–14] aimed at bridging these gaps, by devising new classes of strain energy functions that lead to a more accurate modelling of the multiaxial deformation datasets of a wide range of rubber-like materials, with mechanistically consistent results (i.e. remaining free from the basic ill-posed effects associated with other models for the same datasets). These efforts culminated in a recently proposed *comprehensive* model [15], formulated based on the principal stretches λ_i ($i = 1, 2, 3$) of a non-separable form—see also [16] for more results. In further enhancing those endeavours, a new strain energy function is presented here, based on the principal invariants I_i ($i = 1, 2, 3$) of the (left) Cauchy–Green deformation tensor \mathbf{B} , specialised for application to isotropic incompressible ($I_3 = 1$) soft solids. The proposed model is of the binomial additive form; $W(I_1, I_2) \equiv f(I_1) + g(I_2)$, and is a generalisation of the response functions previously devised by the author (e.g. [17, 18]):

$$W(I_1, I_2) = \sum_{j=1} \frac{3(n_j - 1)}{2n_j} \mu_j N \left[\frac{1}{3N(n_j - 1)} (I_1 - 3)^{\beta_j} - \ln \left(\frac{I_1 - 3N}{3 - 3N} \right)^{\beta_j} \right] + \sum_{k=1} C_k \left[\left(\frac{I_2}{3} \right)^{\epsilon_k} - 1 \right], \quad (1)$$

where:

$$\begin{cases} n_j, \mu_j, N, C_k \in \mathbb{R}^+, \\ \beta_j, \epsilon_k \in \mathbb{R}, \end{cases} \quad (2)$$

are model parameters, and I_1 and I_2 are the first and second principal invariants of \mathbf{B} ($= \mathbf{F}\mathbf{F}^T$), respectively. Note that parameter N controls the limit of extensibility and thus is not subscripted, i.e. is singular valued (see, e.g. [15]). While the general form of the model $W(I_1, I_2)$ in Eq. (1) may be expanded to any number of terms required, here we restrict our attention to the first-term expansion of the model:

$$W(I_1, I_2) = \frac{3(n - 1)}{2n} \mu N \left[\frac{1}{3N(n - 1)} (I_1 - 3)^\beta - \ln \left(\frac{I_1 - 3N}{3 - 3N} \right)^\beta \right] + C_2 \left[\left(\frac{I_2}{3} \right)^\epsilon - 1 \right], \quad (3)$$

to minimise the possible risk of over-prescribing constitutive parameters and thereby the uniqueness issues surrounding the obtained fits and the model parameter values [19]. Accordingly, the one-term form of the model in Eq. (3) contains six model parameters. Note that the coefficient C_2 is so denoted to be in keeping with the classical notation of I_2 terms.

The mathematical underpinnings of the proposed model will be further elaborated in Sect. 2, where a more detailed account of the model background and model parameters will be provided. It will be demonstrated that most of the invariants-based models in the literature are indeed a subset of this model, i.e. the model in Eq. (1) or that in Eq. (3) is the *parent* to most known invariants-based models. In Sect. 3 the application of the model to multiaxial extant experimental data of a diverse range of isotropic incompressible soft solids will be presented, including filled and unfilled rubber specimens, silicone rubber samples, extremely soft, cross-linked and double-network hydrogels, liquid crystal elastomers, and biomaterials, where the favourable agreement between the model predictions and the experimental data will be demonstrated (with relative errors typically below 4%). The unfilled rubber datasets are those of the canonical Treloar [20] and Kawabata et al. [21] on rubber vulcanisates under uniaxial, equi-biaxial and pure shear loadings. Filled rubber datasets are due to Lahellec et al. [22] on uniaxial and simple shear of a commercial filled rubber compound by Michelin, and a filled hydrogenated nitrile butadiene rubber (HNBR) specimen under uniaxial deformation due to Hohenberger et al. [23] with a distinct inflection point in the stress-deformation curve. The silicone rubber datasets are those of Meunier et al. [24] for unfilled specimens under uniaxial tension and compression, equi-biaxial and pure shear deformations, and Jiang et al. [25] on general biaxial and equi-biaxial deformations of a commercial non-reinforced silicone elastomer. Hydrogel datasets are due to Yohsuke et al. [26] and Mai et al. [27] on multiaxial deformation of polyacrylamide (PAAm) and a double-network hydrogels, respectively, as well as that of Saadedine et al. [28] on crossed-linked hydrogel specimens with various amounts of added cross-linkers

² I have borrowed the term ‘standard’ from Dal et al. [10] in this context. Therein they mainly refer to standard methodologies for identification of the constitutive behaviour of rubber-like materials. My focus here is only on the constitutive model.

under uniaxial tension. The fits for liquid crystal elastomers are provided for uniaxial tensile (only) deformation datasets used in [29] originally due to Raistrick et al. [30], that of Tokumoto et al. [31] and the dataset due to Merkel et al. [32] as used in [33]. The datasets pertaining to biomaterial samples are those of Budday et al. [34] on uniaxial tension and compression, and simple shear, deformations of human brain tissue, uniaxial tension–compression of human whole blood clots due to Cahalane et al. [35], and the simple shearing of a thrombus mimic specimen constructed from bovine blood due to Sugerma et al. [36] measuring the normal (to the sheared surface) stress component of simple shear deformation and showing the unusual *reverse* Poynting effect. We note here that the foregoing datasets are either the established barometers for gauging the basic performance of a model (such as those of Treloar [20] and Kawabata et al. [21]), or have proved challenging for the existing models to provide a good fit to as demonstrated in the original cited studies, much less for a single model to provide accurate fits to all these diverse behaviours and datasets. In Sect. 4 some important points of discussion will be conferred in relation to the modelling results, including the *predictions* of other modes of deformation provided by the model for some of the specimens considered here, and issues surrounding the convexity of the iso-energy plots. It is concluded in Sect. 5 that given: (i) the notably low relative errors and markedly high accuracy of the model predictions for the finite deformation of the wide range of soft solids considered here, (ii) simple mathematical form of the model and (iii) the manageable number of model parameters, the proposed model in Eq. (3) may serve as an *a priori standard* choice of hyperelastic strain energy function W with unified applicability for modelling the constitutive behaviour of isotropic incompressible soft solids.

2 The model

The idea behind the proposed model in this manuscript stems from the new class of response functions developed by the author in a preceding paper [17], where a general solution for limiting chain extensibility response was constructed as a [1/1] rational Padé approximant in I_1 of the form:

$$2W_1 \equiv 2 \frac{\partial W}{\partial I_1} = \frac{1}{n} \mu \frac{I_1 - 3nN}{I_1 - 3N}, \quad (4)$$

which leads to the following explicit generalised neo-Hookean strain energy function [13]:

$$W(I_1) = \frac{3(n-1)}{2n} \mu N \left[\frac{1}{3N(n-1)} (I_1 - 3) - \ln \left(\frac{I_1 - 3N}{3 - 3N} \right) \right], \quad (5)$$

subject to $I_1 < 3N$ so that that the $\ln(\blacksquare)$ function remains well defined. Parameter N controls the extensibility limit and has a structural basis akin to the number of Kuhn's segments, n is a parameter which controls the rate of strain hardening, $n, N \in \mathbb{R}^+$, and μ is related to the infinitesimal shear modulus μ_0 through: $\mu = \mu_0 \frac{n(1-N)}{1-nN}$. The favourable agreement between the predictions of this model and the multiaxial deformation data for a range of filled and unfilled rubber specimens was demonstrated in [13]. While the response function in Eq. (4) is an improvement to that of the Gent model [37] which is of [0/1] order in I_1 , a further generalisation of that response function to an order [β /1] may be achieved by, for example, considering:

$$2W_1 = \frac{1}{n} \mu \beta \frac{I_1(I_1 - 3)^{\beta-1} + 3N[1 - (I_1 - 3)^{\beta-1}] - 3nN}{I_1 - 3N}. \quad (6)$$

Note that the ansatz in Eq. (6) is not the only way of achieving a [β /1] rational response function in I_1 ; however, it is a particularly useful one as it may be integrated to give the following compact strain energy function:

$$W(I_1) = \int W_1 dI_1 = \frac{3(n-1)}{2n} \mu N \left[\frac{1}{3N(n-1)} (I_1 - 3)^\beta - \ln \left(\frac{I_1 - 3N}{3 - 3N} \right)^\beta \right]. \quad (7)$$

While in the mathematical sense β is defined to be $\beta \in \mathbb{N}$, from a phenomenological point of view this requirement may be relaxed, so that $\beta \in \mathbb{R}$. That is, considering $\beta \in \mathbb{R}$ does not violate the first of Beatty's [38] empirical inequalities $W_1(I_1) > 0$ so far as the $\ln(\blacksquare)$ function remains well defined; a sufficient condition for which is $I_1 < 3N$.

However, the $W(I_1)$ function in Eq. (7) is still of the generalised neo-Hookean type, and as a result all the usual shortcomings of the generalised neo-Hookean strain energy functions may be extended to this function

too, including the extent of correlation with the data at lower levels of deformation (see, e.g. [39, 40]) and in compliance with the universal relationships of finite elasticity (see, e.g. [18, 41–43]). These shortcomings necessitate the inclusion of an I_2 adjunct term in the strain energy function W . Of the various choices of an I_2 adjunct term that exist in the literature, we devise the general functional from:

$$W(I_2) = C_2 \left[\left(\frac{I_2}{3} \right)^\epsilon - 1 \right], \quad C_2 \in \mathbb{R}^+, \quad \epsilon \in \mathbb{R}. \quad (8)$$

From Eq. (8) it is clear that when $\epsilon = 1$, one gets the classical Mooney–Rivlin I_2 term (the multiplier 3 can be absorbed into the coefficient C_2). Limited use of this functional form, for when $\epsilon = 0.5$, may be seen in the work of Carroll [44], for which a structural underpinning using the tube topological constraint model was provided in [18]. It will be shown in Sect. 3 that, further to the structural motivation, the $W(I_2)$ function in Eq. (8) provides a very useful and flexible addition to the $W(I_1)$ term for accurately capturing the deformation of a wide range of soft solids and deformation ranges.

Remark 1 The second of conditions in Eq. (8), i.e. $\epsilon \in \mathbb{R}$, may lead to the violation of Beatty’s [38] second empirical relationship, namely $W_2 \geq 0$, for when $\epsilon < 0$. However, we have deliberately *not* restricted ϵ to $\epsilon \in \mathbb{R}^+$, since as it will be shown and discussed later, this condition will unnecessarily lead to excluding the prediction of the *reverse* Poynting effect in some applications. This occurrence has also been discussed at length, and reconciled with, by Mihai and Goriely [45]. In that spirit, we do not opt for the overtly restrictive $\epsilon \in \mathbb{R}^+$, and instead consider the condition as laid out in Eq. (8).

What remains to do now is to construct the final form of the $W(I_1, I_2)$ function, which we consider as a binomial additive form of $W(I_1, I_2) \equiv f(I_1) + g(I_2)$, with the functions f and g defined in Eqs. (7) and (8), respectively, to arrive at the model in Eq. (3):

$$W = \frac{3(n-1)}{2n} \mu N \left[\frac{1}{3N(n-1)} (I_1 - 3)^\beta - \ln \left(\frac{I_1 - 3N}{3 - 3N} \right)^\beta \right] + C_2 \left[\left(\frac{I_2}{3} \right)^\epsilon - 1 \right], \quad I_1 < 3N,$$

subject to the foregoing conditions on parameters n , N , β , C_2 and ϵ . Note that the infinitesimal shear modulus μ_0 for this model is:

$$\mu_0 = 2[W_1(I_1 = 3) + W_2(I_2 = 3)] \Rightarrow \mu_0 = \frac{\mu\beta N}{n} \frac{1-n}{1-N} + \frac{2\epsilon}{3} C_2, \quad (9)$$

and that μ and C_2 are stress-like parameters while n , N , β and ϵ are dimensionless.

Remark 2 Structurally, parameter N ought to be positive (> 0). However, from a phenomenological point of view, so long as μ_0 remains positive and the first of empirical relationships (i.e. $W_1 > 0$) is not violated, there is no reason as to why parameters N and n need to be restricted to \mathbb{R}^+ space. Indeed, applications may be found where N , or both N and n , may assume a negative value. One such application has been presented in [16], and three examples will be presented herein too.

In total, therefore, this model contains six model parameters, and as such is within the territory identified by Ogden et al. [19], i.e. prone to non-uniqueness issues surrounding the obtained fits and model parameter values. While, as will be shown in Sect. 3, this model provides favourable fits to the wide range of soft solid materials and deformations considered here, it may still be judicious in some applications to expand the number of model terms and use the multi-term form of the model as given in Eq. (1). Such applications were not encountered by the author and will not be pursued here.

Before we proceed, it may be informative to demonstrate that our proposed model is the *parent* to most invariants-based (I_1, I_2) models in the literature.³ Accordingly, some examples are demonstrated in the following:

1. Starting with the classical neo-Hookean model, we note that by setting $C_2 = 0$ and $\beta = 1$, in limits when $N \rightarrow \infty$ or $n \rightarrow 1$, we obtain:

$$\lim_{N \rightarrow \infty} W = \lim_{n \rightarrow 1} W = \frac{1}{2} \mu (I_1 - 3). \quad (10)$$

³ Known to the author.

2. Similarly, the polynomial form of the neo-Hookean model is obtained by considering the multi-term model in Eq. (1) and using the same settings, i.e. $\beta_j = j$ and $C_k = 0$:

$$\lim_{n \rightarrow 1} W = \sum_{j=1}^{\infty} \frac{1}{2} \mu_j (I_1 - 3)^j. \quad (11)$$

The relationship in Eq. (11) covers many of the power-series combination of $(I_1 - 3)^j$ such as Yeoh's cubic model [46] etc.

3. Models based on fractional powers of $(I_1 - 3)$ term(s) are also a subset of the proposed model, demonstrable using the same procedure as that in the foregoing. For example, by setting $C_k = 0$ and $\beta_1 = 1$ and $\beta_2 = \frac{3}{4}$, we obtain at the limit $n \rightarrow 1$:

$$\lim_{n \rightarrow 1} W = \frac{1}{2} \left[\mu_1 (I_1 - 3) + \mu_2 (I_1 - 3)^{\frac{3}{4}} \right], \quad (12)$$

which is a model proposed by Nunes in [47]. This fractional-power expansion of $(I_1 - 3)$ terms also becomes close to the functional form of the model by Lopez-Pamies [48].

4. Another model readily recoverable from that in Eq. (3) is the seminal Mooney–Rivlin model. By setting $\beta = \epsilon = 1$ and at the limit $N \rightarrow \infty$ or $n \rightarrow 1$ we get: which is the Mooney–Rivlin model on noting that the C_2 coefficient in (13) is equal to $3C_2$ of that in the former model.

$$\lim_{N \rightarrow \infty} W = \lim_{n \rightarrow 1} W = \frac{1}{2} \mu (I_1 - 3) + C_2 \left(\frac{I_2}{3} - 1 \right), \quad (13)$$

5. In the limit $n \rightarrow \infty$ and setting $\beta = 1$ and $C_2 = 0$ we have from Eq. (3):

$$\lim_{n \rightarrow \infty} W = -\frac{3}{2} N \mu \ln \left(-\frac{I_1 - 3N}{3N - 3} \right). \quad (14)$$

We also note from Eq. (9) that:

$$\lim_{n \rightarrow \infty, \beta=1, C_2=0} \left(\frac{\mu N}{n} \frac{1-n}{1-N} \right) = \frac{\mu N}{N-1} = \mu_0, \quad (15)$$

which renders the relationship in Eq. (14) as:

$$\lim_{n \rightarrow \infty} W = -\frac{3}{2} \mu_0 (N-1) \ln \left(-\frac{I_1 - 3N}{3N - 3} \right). \quad (16)$$

By setting the limiting chain extensibility parameter J_m in the Gent model as: $J_m = 3N - 3$, Eq. (16) can be re-written as:

$$\lim_{n \rightarrow \infty} W = -\frac{1}{2} J_m \mu_0 \ln \left(1 - \frac{I_1 - 3}{J_m} \right), \quad (17)$$

which is the well-known Gent model [37].

6. On using the multi-term form of the model in Eq. (1), and by setting $\beta_1 = 1$ and $\beta_2 = 4$, and $\epsilon_1 = \frac{1}{2}$, we obtain in limits $N \rightarrow \infty$ and $n_1, n_2 \rightarrow 1$:

$$\lim_{N \rightarrow \infty, n_1, n_2 \rightarrow 1} W = \frac{1}{2} \mu_1 (I_1 - 3) + \frac{1}{2} \mu_2 (I_1 - 3)^4 + C_1 \left[\sqrt{\frac{I_2}{3}} - 1 \right], \quad (18)$$

i.e. the model by Carroll [44] with the change of notation $A = \frac{1}{2} \mu_1$, $B = \frac{1}{2} \mu_2$ and $C = C_1$.

7. Though trivial, we note that earlier subsets of the model in Eq. (3) will be retrieved by setting $\beta = 1$ and $C_2 = 0$, which directly reproduces the model used in [13], and by further setting $n = 3$ the model in [49] and [50] is obtained.

More examples may also be recounted; however, we stop here in the interest of concision.

3 Correlation with experimental data

With the mathematical background of the model set out in the previous section, we now proceed to demonstrate the application of the model to the finite deformation of a wide range of soft solids, from filled and unfilled rubber specimens to hydrogels, liquid crystal elastomers and biomaterials. The considered experimental datasets pertaining to these specimens contain various multiaxial deformation modes including uniaxial, (equi-)biaxial, pure and simple shear deformations. Accordingly, we first derive and present the relevant stress—deformation relationships.

3.1 Stress—deformation relationships

The Cauchy stress \mathbf{T} for an isotropic incompressible material is given by:

$$\mathbf{T} = -p\mathbf{I} + 2W_1\mathbf{B} - 2W_2\mathbf{B}^{-1}, \quad (19)$$

where \mathbf{B} ($=\mathbf{F}\mathbf{F}^T$) is the left Cauchy–Green deformation tensor and \mathbf{B}^{-1} is its inverse, p is the arbitrary Lagrange multiplier enforcing the condition of incompressibility, \mathbf{I} is the identity tensor, and W_1 and W_2 are the partial derivatives of the strain energy function W with respect to the first and second principal invariants of \mathbf{B} . These are defined as:

$$I_1 = \lambda_1^2 + \lambda_2^2 + \lambda_3^2, \quad I_2 = \lambda_1^{-2} + \lambda_2^{-2} + \lambda_3^{-2}, \quad (20)$$

with $I_3 = 1$ due to incompressibility: $\lambda_1\lambda_2\lambda_3 = 1$.

It follows that, using the assumption of plane stress ($T_{33} = 0$), for uniaxial deformations where $\lambda_1 = \lambda$ and $\lambda_2 = \lambda_3 = \lambda^{-0.5}$, from model (3) we will have:

$$T_{uni} = \frac{\mu\beta}{n} \frac{I_1(I_1 - 3)^{\beta-1} + 3N[1 - (I_1 - 3)^{\beta-1}] - 3nN}{I_1 - 3N} \left(\lambda^2 - \frac{1}{\lambda} \right) + \frac{2C_2\epsilon}{3^\epsilon} I_2^{\epsilon-1} \left(\lambda - \frac{1}{\lambda^2} \right), \quad (21)$$

where $I_1 = \lambda^2 + 2\lambda^{-1}$ and $I_2 = 2\lambda + \lambda^{-2}$. The equivalent nominal stress \mathbf{P} components may be obtained from \mathbf{T} on using the conversion: $\mathbf{T} = \mathbf{F}\mathbf{P}$, where \mathbf{F} is the deformation gradient tensor, which results in:

$$P_{uni} = \frac{\mu\beta}{n} \frac{I_1(I_1 - 3)^{\beta-1} + 3N[1 - (I_1 - 3)^{\beta-1}] - 3nN}{I_1 - 3N} \left(\lambda - \frac{1}{\lambda^2} \right) + \frac{2C_2\epsilon}{3^\epsilon} I_2^{\epsilon-1} \left(1 - \frac{1}{\lambda^3} \right). \quad (22)$$

Similarly, in equi-biaxial deformations where $\lambda_1 = \lambda_2 = \lambda$ and $\lambda_3 = \lambda^{-2}$ we find using the model in Eq. (3):

$$\begin{cases} T_{eq-bi} = \frac{\mu\beta}{n} \frac{I_1(I_1 - 3)^{\beta-1} + 3N[1 - (I_1 - 3)^{\beta-1}] - 3nN}{I_1 - 3N} \left(\lambda^2 - \frac{1}{\lambda^4} \right) + \frac{2C_2\epsilon}{3^\epsilon} I_2^{\epsilon-1} \left(\lambda^4 - \frac{1}{\lambda^2} \right), \\ P_{eq-bi} = \frac{\mu\beta}{n} \frac{I_1(I_1 - 3)^{\beta-1} + 3N[1 - (I_1 - 3)^{\beta-1}] - 3nN}{I_1 - 3N} \left(\lambda - \frac{1}{\lambda^5} \right) + \frac{2C_2\epsilon}{3^\epsilon} I_2^{\epsilon-1} \left(\lambda^3 - \frac{1}{\lambda^3} \right), \end{cases} \quad (23)$$

with $I_1 = 2\lambda^2 + \lambda^{-4}$ and $I_2 = \lambda^4 + 2\lambda^{-2}$. For general biaxial deformations in directions 1 and 2, these relationships become:

$$\begin{cases} (T_{bi})_1 = \frac{\mu\beta}{n} \frac{I_1(I_1 - 3)^{\beta-1} + 3N[1 - (I_1 - 3)^{\beta-1}] - 3nN}{I_1 - 3N} \left(\lambda_1^2 - \frac{1}{\lambda_1^3\lambda_2^2} \right) + \frac{2C_2\epsilon}{3^\epsilon} I_2^{\epsilon-1} \left(\lambda_1^2\lambda_2^2 - \frac{1}{\lambda_1^3} \right), \\ (T_{bi})_2 = \frac{\mu\beta}{n} \frac{I_1(I_1 - 3)^{\beta-1} + 3N[1 - (I_1 - 3)^{\beta-1}] - 3nN}{I_1 - 3N} \left(\lambda_2^2 - \frac{1}{\lambda_1^2\lambda_2^3} \right) + \frac{2C_2\epsilon}{3^\epsilon} I_2^{\epsilon-1} \left(\lambda_1^2\lambda_2^2 - \frac{1}{\lambda_2^3} \right), \end{cases} \quad (24)$$

where $I_1 = \lambda_1^2 + \lambda_2^2 + (\lambda_1\lambda_2)^{-2}$ and $I_2 = \lambda_1^{-2} + \lambda_2^{-2} + (\lambda_1\lambda_2)^2$. The equivalent stress components in terms of the nominal stress P are:

$$\begin{cases} (P_{bi})_1 = \frac{\mu\beta}{n} \frac{I_1(I_1 - 3)^{\beta-1} + 3N[1 - (I_1 - 3)^{\beta-1}] - 3nN}{I_1 - 3N} \left(\lambda_1 - \frac{1}{\lambda_1^3\lambda_2^2} \right) + \frac{2C_2\epsilon}{3^\epsilon} I_2^{\epsilon-1} \left(\lambda_1\lambda_2^2 - \frac{1}{\lambda_1^3} \right), \\ (P_{bi})_2 = \frac{\mu\beta}{n} \frac{I_1(I_1 - 3)^{\beta-1} + 3N[1 - (I_1 - 3)^{\beta-1}] - 3nN}{I_1 - 3N} \left(\lambda_2 - \frac{1}{\lambda_1^2\lambda_2^3} \right) + \frac{2C_2\epsilon}{3^\epsilon} I_2^{\epsilon-1} \left(\lambda_1^2\lambda_2 - \frac{1}{\lambda_2^3} \right). \end{cases} \quad (25)$$

For the pure shear deformation where $\lambda_1 = \lambda$, $\lambda_2 = 1$ and $\lambda_3 = \lambda^{-1}$, the model in Eq. (3) gives:

$$\begin{cases} T_{ps} = \left\{ \frac{\mu\beta}{n} \frac{I_1(I_1-3)^{\beta-1} + 3N[1-(I_1-3)^{\beta-1}] - 3nN}{I_1-3N} + \frac{2C_2\epsilon}{3^\epsilon} I_2^{\epsilon-1} \right\} \left(\lambda^2 - \frac{1}{\lambda^2} \right), \\ P_{ps} = \left\{ \frac{\mu\beta}{n} \frac{I_1(I_1-3)^{\beta-1} + 3N[1-(I_1-3)^{\beta-1}] - 3nN}{I_1-3N} + \frac{2C_2\epsilon}{3^\epsilon} I_2^{\epsilon-1} \right\} \left(\lambda - \frac{1}{\lambda^3} \right), \end{cases} \quad (26)$$

with $I_1 = I_2 = \lambda^2 + 1 + \lambda^{-2}$. Finally, for the case of simple shear, where the deformation gradient is defined by:

$$\mathbf{F} = \begin{bmatrix} 1 & \gamma & 0 \\ \gamma & 1 & 0 \\ 0 & 0 & 1 \end{bmatrix}, \quad (27)$$

with γ being the amount of shear, the shear component of the Cauchy stress is computed via:

$$T_{ss} = 2\gamma(W_1 + W_2), \quad (28)$$

which on using model (3) results in:

$$\begin{cases} T_{ss} = \left\{ \frac{\mu\beta}{n} \frac{I_1(I_1-3)^{\beta-1} + 3N[1-(I_1-3)^{\beta-1}] - 3nN}{I_1-3N} + \frac{2C_2\epsilon}{3^\epsilon} I_2^{\epsilon-1} \right\} \gamma, \\ P_{ss} = \left\{ \frac{\mu\beta}{n} \frac{I_1(I_1-3)^{\beta-1} + 3N[1-(I_1-3)^{\beta-1}] - 3nN}{I_1-3N} + \frac{2C_2\epsilon}{3^\epsilon} I_2^{\epsilon-1} \right\} \frac{\gamma}{\frac{\gamma}{2} + \sqrt{1 + \frac{\gamma^2}{4}}}, \end{cases} \quad (29)$$

where $I_1 = I_2 = 3 + \gamma^2$.

Depending on the source experimental data, either the Cauchy T or nominal P stress—deformation relationships summarised in the foregoing will be used for fitting with the data in the sequel.

3.2 The fitting process

In keeping with the source data, the majority of the fittings here were carried in the engineering space (i.e. in $P - \lambda$ domain), with the exception of some datasets that were originally presented in the Cauchy space. We note that other domains also exist, such as the generalised Mooney space [51], which facilitate obtaining robust fits; however, they are not well-versed in the literature. The fitting process used here is similar to that used in our previous studies [12–16]. Concisely, either the nominal P or Cauchy T stress—deformation relationships in Eqs. (21) to (26) and (29) were simultaneously fitted to the relevant deformation modes from each considered dataset. The best fit was sought by minimising the residual sum of squares (RSS) function defined as: $RSS = \sum_r (P^{\text{model}} - P^{\text{experiment}})_r^2$, or equivalently in terms of the Cauchy stress as $RSS = \sum_r (T^{\text{model}} - T^{\text{experiment}})_r^2$, where r is the number of data points. This minimisation was performed via an in-house developed code in MATLAB[®], using the genetic algorithm (GA) function. The coefficient of determination R^2 values are reported as a measure of the goodness of the obtained fits, as well as the ensuing relative error (%) calculated as: $\left| \frac{P^{\text{model}} - P^{\text{experiment}}}{P^{\text{experiment}}} \right| \times 100$ or equivalently $\left| \frac{T^{\text{model}} - T^{\text{experiment}}}{T^{\text{experiment}}} \right| \times 100$. Note that the data point (λ, P) at the undeformed state, i.e. (1,0), was removed from each dataset before the start of the fitting process to preclude any potential numerical instability that may arise from values of $\beta < 1$, i.e. to avoid division by zero at point $\lambda = 1$ (corresponding to $P, T = 0$) in stress—deformation relationships.

3.3 Fitting results

Using the mathematical relationships and the fitting procedure described, we now present the modelling results in respect of each class of soft materials considered.

Table 1 Model parameter values for unfilled rubber vulcanisate specimens due to Treloar [20] and Kawabata et al. [21]

| | Treloar data [20] | | | | | | |
|--------------|---------------------------|---------|---------|-------------|-------------|----------------|-------------------|
| | μ [MPa] | N [-] | n [-] | β [-] | C_2 [MPa] | ϵ [-] | R^2 |
| Uniaxial | 0.39 | 26.60 | 4.93 | 0.69 | 0.30 | 0.41 | 0.99 ₉ |
| Equi-biaxial | | | | | | | 0.99 ₉ |
| Pure shear | | | | | | | 0.99 ₉ |
| | Kawabata et al. data [21] | | | | | | |
| | μ [MPa] | N [-] | n [-] | β [-] | C_2 [MPa] | ϵ [-] | R^2 |
| Uniaxial | 0.25 | 0.68 | 0.89 | 1.00 | 0.20 | 0.47 | 0.99 ₉ |
| Equi-biaxial | | | | | | | 0.99 ₉ |
| Pure shear | | | | | | | 0.99 ₈ |

3.3.1 Unfilled rubber

It has become customary, when comparing the ability of the existing models in the literature, to gauge the accuracy and predictability of the models against the canonical experimental data of Treloar [20] and Kawabata et al. [21] on multiaxial deformation of unfilled rubber vulcanisates. The former dataset pertains to vulcanised sulphur (8%) rubber, and the latter is that of vulcanised isoprene rubber samples. Accordingly, the relationships in Eqs. (22), (23)₂ and (26)₂ were simultaneously fitted to the uniaxial, equi-biaxial and pure shear deformation datasets of each study. The tabulated numerical datapoints for these datasets can be found in [50] and [21], respectively. The model parameter values for each dataset are presented in Table 1, and the fitting results are illustrated in Figs. 1 and 2. The R^2 values for both datasets are in excess of 0.99₈, underlining the favourability of the model correlation with the two canonical datasets.

Starting by Treloar's data [20] for natural rubber vulcanisates, from the plots in Fig. 1 it is clear that the model captures the data most favourably, with the relative errors remaining below 4% across most of the deformation domain, except for the very small deformation levels at the beginning of deformation (i.e. in the vicinity of $\lambda = 1$). With these reassuring results, we move to the data due to Kawabata et al. [21], presented in Fig. 2.

Similar to the results pertaining to Treloar's natural rubber vulcanisate specimens, the multiaxial data of unfilled isoprene rubber vulcanisates due to Kawabata et al. [21] also correlate favourably with the model predictions. The relative error plots in Fig. 2 indicate that the values of relative error are again typically below 4% across the whole of the deformation domain, except for the small levels around $\lambda = 1$ at the beginning of the deformation. These two canonical datasets provide a reassuring first step in showcasing the ability of the proposed model for an accurate application to the finite deformation of rubbers.

3.3.2 Filled rubber

Filled rubbers exhibit a distinctly different deformation behaviour than their unfilled counterparts. The introduction of the filler particles is known to *distort* the mechanical behaviour of the filled rubbers, and this distortion becomes more pronounced with higher levels of filler [23]. Examples include a shear softening behaviour; e.g. a downward concavity at low deformations in deformation curves, thought to be associated with the breakage of filler network [23], and the Payne effect [52], which in severe cases reflects itself as an inflection point in uniaxial tension and/or compression curves [23]. These behaviours have proved to be challenging to capture for most of the existing models in the literature⁴—see, e.g. [16, 23] and [53] for some comparative examples. Here, we present the application of our proposed model to exemplar datasets which highlight the aforementioned two behaviours, i.e. the shear softening and the Payne effect. For the former, we consider the multiaxial deformation dataset of Lahellec et al. [22] involving uniaxial and simple shearing of a commercial filled rubber compound developed by the Michelin tyres, and for the latter we use the data due to Hohenberger et al. [23] on uniaxial tension and compression of a filled hydrogenated nitrile butadiene rubber (HNBR) sample. Accordingly, in keeping with the source data, the relationships in Eqs. (22) and (29)₂ were fitted to each dataset. The tabulated numerical datapoints for these datasets, extracted from the foregoing

⁴ A notable exception is that of Lopez-Pamies [48].

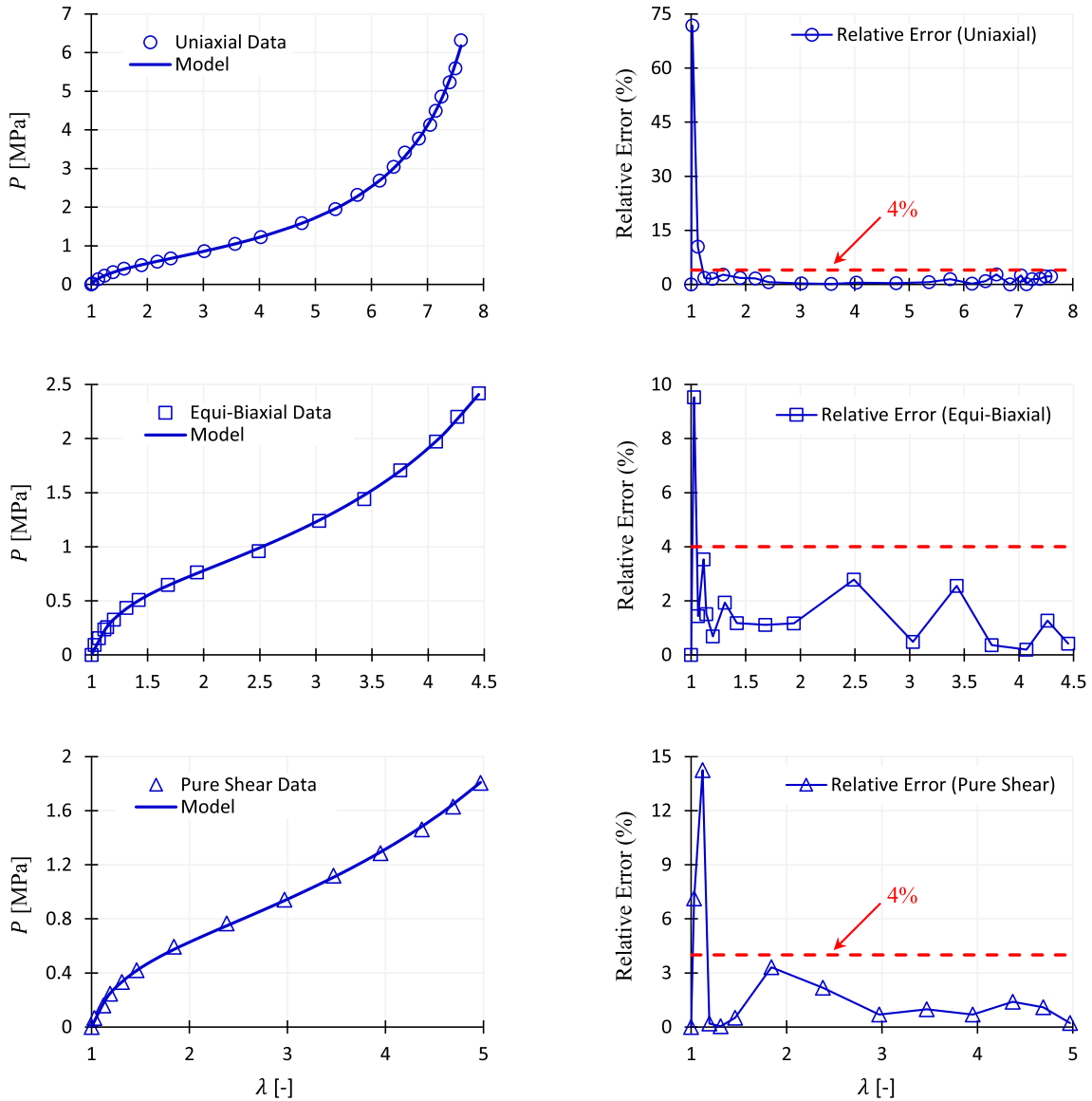


Fig. 1 Modelling results versus the experimental data due to Treloar [20] for unfilled natural rubber vulcanisates under uniaxial, equi-biaxial and pure shear deformations. The panels on the right show the relative errors. The dotted (red) lines mark the error level at 4% (see the on-line version for plots in colour)

studies, have been summarised in Appendix A, Tables 9 and 10. The obtained model parameter values are presented in Table 2, and the fitting results are illustrated in Figs. 3 and 4. The R^2 values for both datasets are in excess of 0.999, indicative of the capability of the model in capturing such challenging mechanical behaviours.

As the stress—deformation plot in Fig. 3 indicates, the compression—tension behaviour of the considered filled rubber specimen (HNBR) is highly asymmetrical. The inflection point at compressive stretch is also noticeable. The model provides a favourable fit, and successfully captures these challenging behaviours. The relative errors plot also indicates that, similar to the considered unfilled rubber datasets in the previous section, the relative errors remain typically below 4% for most of the deformation range, except within very small deformations around $\lambda = 1 \pm 0.1$.

The plots in Fig. 4 demonstrate the modelling results for the commercial filled rubber data due to Lahellec et al. [22] under uniaxial and simple shear deformations. Reassuringly, the ensuing relative errors remain under

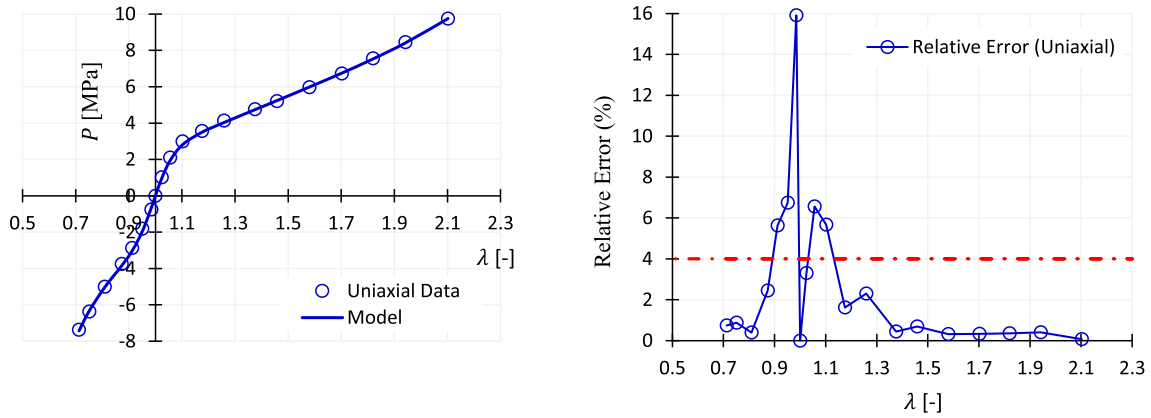


Fig. 3 Modelling results versus the experimental data due to Hohenberger et al. [23] for a filled rubber specimen (HNBR) under uniaxial tension and compression. The panels on the right show the relative errors. The dotted (red) line marks the error level at 4% (see the on-line version for plots in colour)

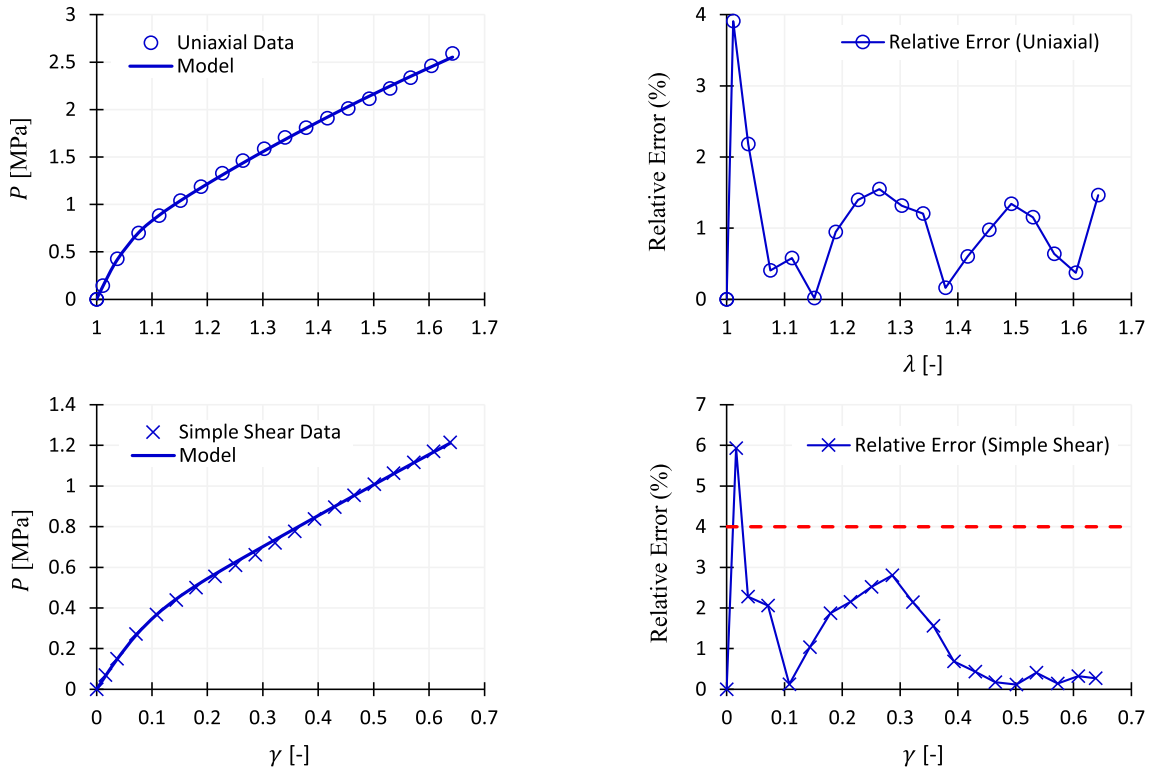


Fig. 4 Modelling results versus the experimental data due to Lahellec et al. [22] for a commercial filled rubber compound developed by the Michelin under uniaxial and simple shear deformations. The panels on the right show the relative errors. The dotted (red) line marks the error level at 4% (see the on-line version for plots in colour)

4% again (except for very small amounts of initial shearing), and the model is seen to successfully capture the softening behaviour (downward concavity).

The combined results of the previous and current sections highlight that the proposed model in Eq. (3) offers the capability to accurately capture the finite deformation behaviour of both filled and unfilled rubbers, using a unified model. This is an attractive possibility given the current choice of models in the literature, where most struggle to model the behaviour of both types of materials.

3.3.3 Silicone rubber

Although (unreinforced) silicone rubbers appear to exhibit a fairly standard behaviour under finite deformations, some studies [25, 48, 50] have highlighted the shortcomings of the existing models in providing an accurate fit to such datasets. Accordingly, here we consider the following two datasets on multiaxial deformation of silicone rubber specimens. The first dataset is due to Meunier et al. [24] on an unfilled compound, under uniaxial compression and tension, equi-biaxial and pure shear deformations. The second dataset is due to Jiang et al. [25] on a commercial non-reinforced silicone elastomer under both equi- and general-biaxial deformations. The significance of this dataset is that general biaxial tests, as opposed to equi-biaxial tests, circumvent the promulgation of what is known as *collinearity* in regression (i.e. fitting a model to the data) which hinders obtaining unique model parameter values [54, 55].

The relationships in Eqs. (22), (23)₂ and (26)₂ were simultaneously fitted the dataset of Meunier et al. [24], and Eqs. (23)₂ and (25) were fitted simultaneously to that of Jiang et al. [25]. The tabulated numerical datapoints for these datasets, collated from the foregoing studies, have been summarised in Appendix A, Tables 11 and 12. The obtained model parameters are presented in Table 3, and the fitting results are illustrated in Figs. 5 and 6. The R^2 values are in excess of 0.99₄, signalling the ability of the model in capturing the finite deformation behaviour of the considered silicone rubber specimens.

While the typical relative errors for this dataset (typically below 8%) is higher than the preceding examples, the model provides a noticeable improvement in the fits compared with many of the existing models in the literature to this dataset (see, e.g. [48, 50]). The main episode of increased errors is related to the small deformations under pure shear ($\lambda < 1.2$). Overall, however, the model provides a favourable fit, with R^2 values > 0.99.

Table 3 Model parameter values for silicone rubber specimens due to Meunier et al. [24] and Jiang et al. [25]

| | Meunier et al. data [24] | | | | | | |
|-----------------|--------------------------|---------|---------|-------------|-------------|----------------|-------------------|
| | μ [MPa] | N [–] | n [–] | β [–] | C_2 [MPa] | ϵ [–] | R^2 |
| Uniaxial | | | | | | | 0.99 ₉ |
| Equi-biaxial | 0.25 | 3.70 | 1.67 | 1.00 | 2.61 | 0.02 | 0.99 ₉ |
| Pure shear | | | | | | | 0.99 ₄ |
| | Jiang et al. data [25] | | | | | | |
| | μ [kPa] | N [–] | n [–] | β [–] | C_2 [kPa] | ϵ [–] | R^2 |
| Equi-biaxial | 357.93 | – 10.59 | – 8.14 | 1.51 | 252.92 | – 1.14 | 0.99 ₇ |
| General biaxial | | | | | | | 0.99 ₅ |

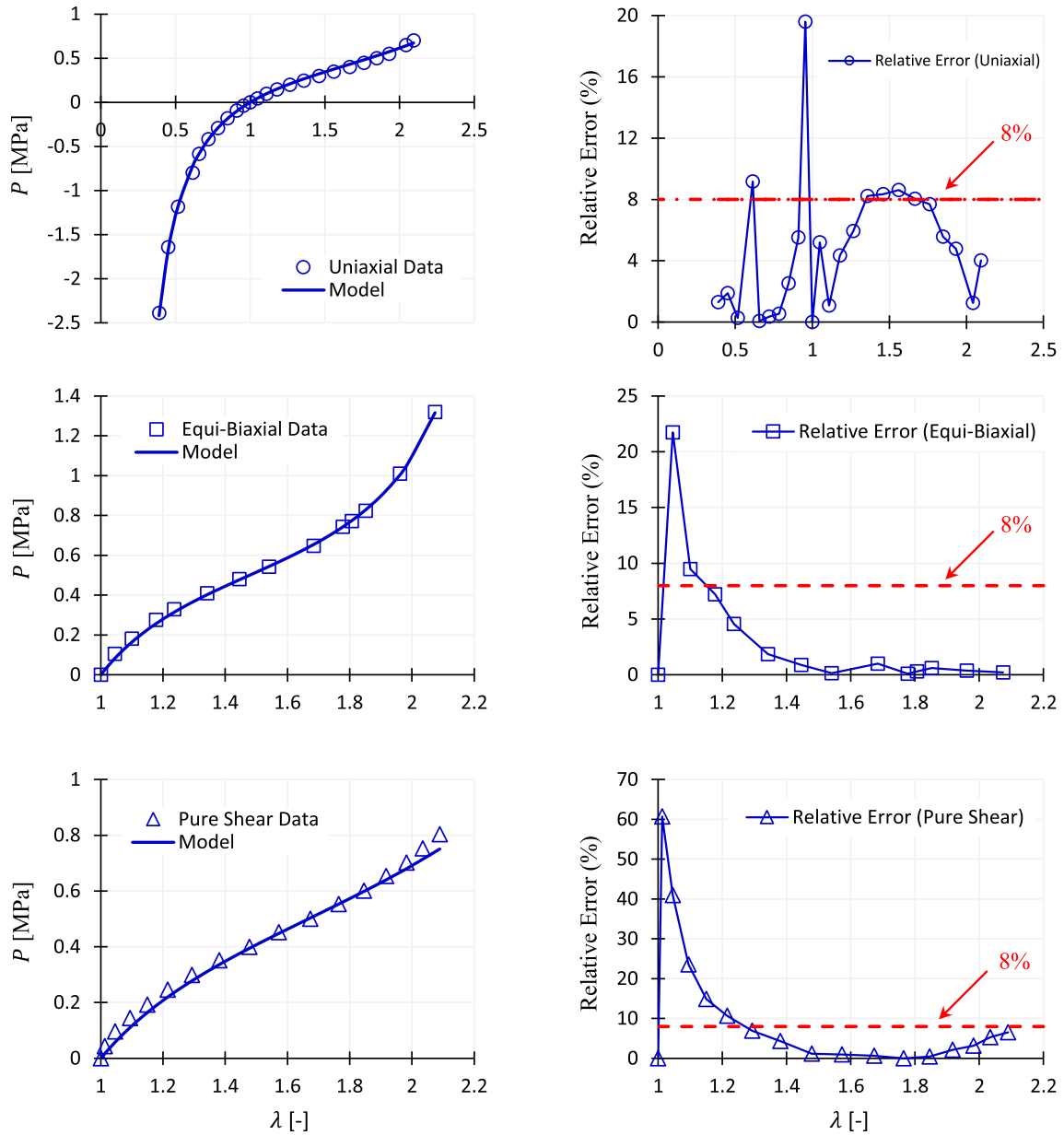


Fig. 5 Modelling results versus the experimental data due to Meunier et al. [24] for an unfilled silicone rubber compound under uniaxial, equi-biaxial and pure shear deformations. The panels on the right show the relative errors. The dotted (red) lines mark the error level at 8% (see the on-line version for plots in colour)

The plots in Fig. 6 provide the modelling results for the dataset due to Jiang et al. [25]. In keeping with the previous datasets, here the relative errors are again below the typical 4%, except for the very small deformation levels at the beginning.

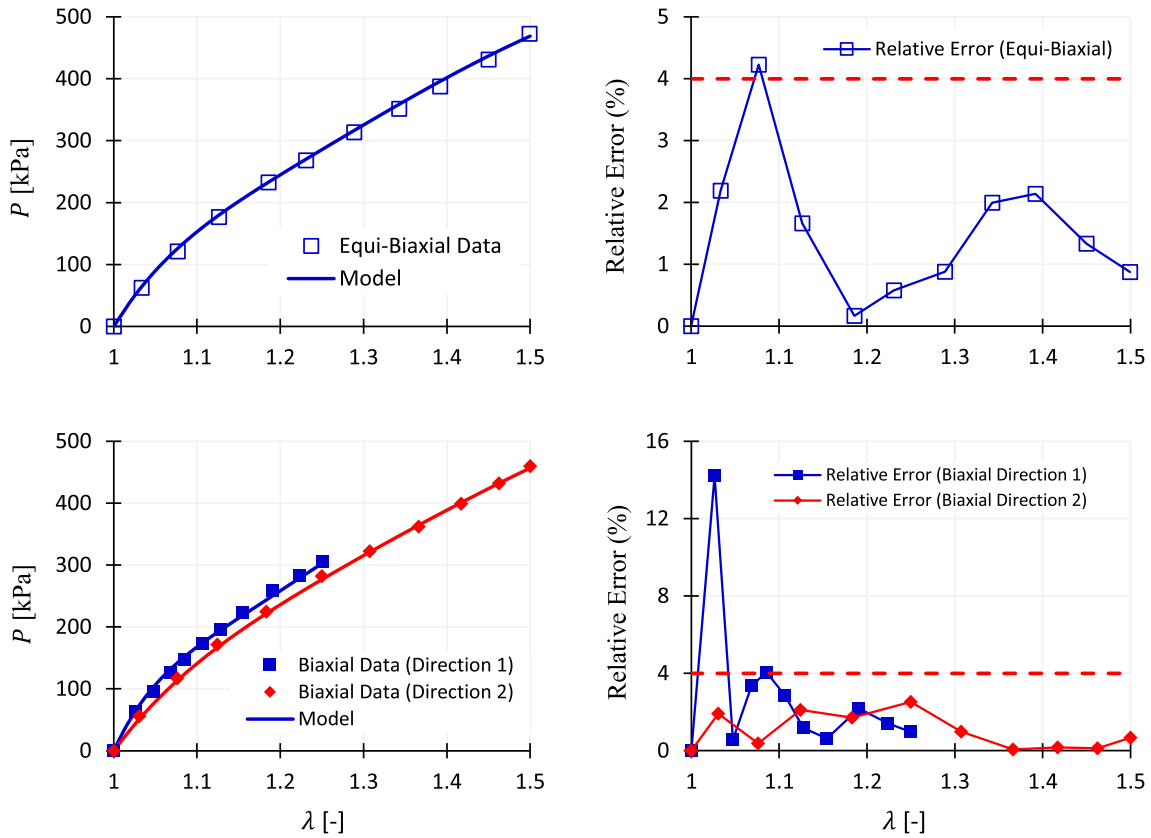


Fig. 6 Modelling results versus the experimental data due to Jiang et al. [25] for a commercial non-reinforced silicone elastomer under equi-biaxial and general biaxial deformations. The panels on the right show the relative errors. The dotted (red) lines mark the error level at 4% (see the on-line version for plots in colour)

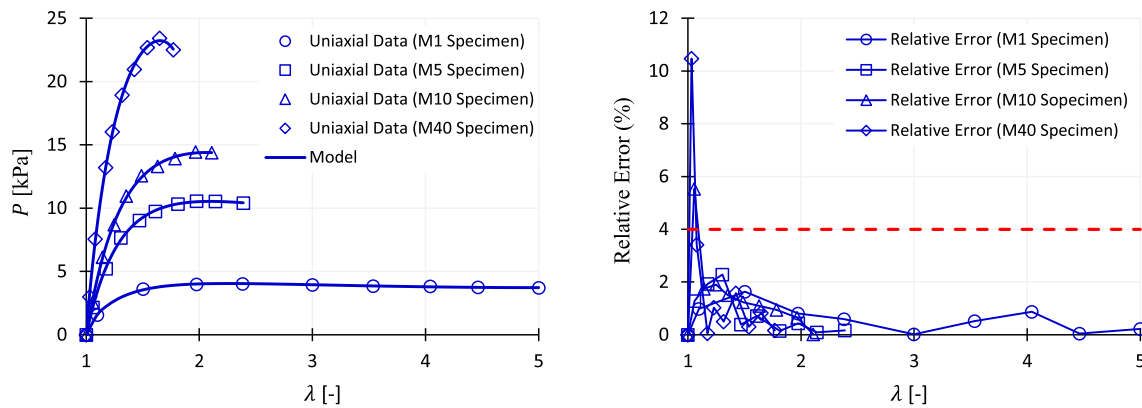
3.3.4 Hydrogels

Modelling the mechanical behaviour of hydrogels has gained a renewed attention, given their wide range of applicability in, for example, biomedical functions (as a medium for 3D cell culture, in situ tissue formation etc.), and due to the fact that their mechanical properties are tuneable, i.e. by changing the cross-link density or water content etc. However, because of their (extreme) softness, modelling their behaviour under finite deformations is not a trivial task. To showcase the capability of the proposed model for capturing the deformation behaviour of these elastomers too, here we consider three datasets pertaining to: (i) a pure hydrogel compound reinforced with various amounts of crosslinkers under uniaxial deformation due to Saadedine et al. [28]; (ii) extremely soft polyacrylamide (PAAm) hydrogel specimens under multiaxial deformation due to Yohsuke et al. [26]; and (iii) a double-network ‘tough’ hydrogel specimen under multiaxial deformation due to Mai et al. [27]. The tabulated numerical datapoints extracted from [28] have been given in [16], and those from [26] and [27] are presented in Tables 13 and 14 of Appendix A.

Starting by the reinforced hydrogel samples of Saadedine et al. [28] with various amount of crosslinkers, here we use the same naming convention for the specimens (i.e. M1, M5, M10 and M40), which indicates the number of milligrams of the contained crosslinker. Equation (22) was fitted to each dataset. Table 4 shows the ensuing model parameter values, and the plots in Fig. 7 illustrate the fitting results. The model provides a favourable fit to the data, with R^2 values in excess of 0.99₉ across all samples, from the softest (i.e. M1 with the lowest amount of crosslinker) to the hardest (i.e. M40 with the highest amount of crosslinker) samples. Note that the table also contains the corresponding value of the infinitesimal shear modulus μ_0 for each sample, calculated from the obtained model parameters on using Eq. (9). Reassuringly, with increase in crosslinks, the calculated shear modulus μ_0 also increases.

Table 4 Model parameter values for the pure hydrogel samples with various amounts of crosslinkers due to Saadedine et al. [28]

| | μ [kPa] | N [–] | n [–] | β [–] | C_2 [kPa] | ϵ [–] | R^2 | μ_0 [kPa] |
|--------------|-------------|---------|---------|-------------|-------------|----------------|-------------------|---------------|
| M1 specimen | 0.76 | 19.42 | 1.10 | 0.58 | 10.51 | 0.63 | 0.99 ₉ | 4.48 |
| M5 specimen | 0.61 | 51.92 | 0.17 | 1.00 | 45.50 | 0.44 | 0.99 ₉ | 10.22 |
| M10 specimen | 0.61 | 8.21 | 0.18 | 1.13 | 68.48 | 0.43 | 0.99 ₉ | 15.86 |
| M40 specimen | 1.52 | 1.71 | 0.715 | 0.83 | 91.60 | 0.55 | 0.99 ₉ | 32.22 |

**Fig. 7** Modelling results versus the experimental data due to Saadedine et al. [28] for a pure hydrogel compound reinforced with various amounts of crosslinkers under uniaxial deformation. The panels on the right show the relative errors. The dotted (red) line marks the error level at 4% (see the on-line version for plots in colour)**Table 5** Model parameter values for soft PAAm and double-network ‘tough’ hydrogel specimens due to Yohsuke et al. [26] and Mai et al. [27], respectively

| | Yohsuke et al. data [26] | | | | | | |
|--------------|--------------------------|--------------------|---------|-------------|-------------|----------------|-------------------|
| | μ [kPa] | N [–] | n [–] | β [–] | C_2 [kPa] | ϵ [–] | R^2 |
| Uniaxial | 4.51 | 17.07 ₅ | 4.23 | 0.94 | 2.91 | 0.57 | 0.99 ₉ |
| Equi-biaxial | | | | | | | 0.99 ₉ |
| Pure shear | | | | | | | 0.99 ₉ |
| | Mai et al. data [27] | | | | | | |
| | μ [MPa] | N [–] | n [–] | β [–] | C_2 [MPa] | ϵ [–] | R^2 |
| Uniaxial | 0.86 | – 0.61 | 10.15 | 1.05 | 0.10 | – 3.92 | 0.99 ₅ |
| Equi-biaxial | | | | | | | 0.99 ₄ |
| Pure shear | | | | | | | 0.99 ₉ |

As the plots in Fig. 7 show, the character of the stress—deformation curves changes with the increase in the amount of crosslinker. However, the model is seen to be well capable of capturing those different curve shapes, with the typical relative errors of below 4% again. With these reassuring results, we proceed with the other two hydrogel datasets in the following.

Next we consider the dataset due to Yohsuke et al. [26] on (extremely) soft polyacrylamide (PAAm) hydrogel specimens, and that of Mai et al. [27] on double-network ‘tough’ hydrogel samples, under uniaxial, equi-biaxial and pure shear deformations. Accordingly, Eqs. (22), (23)₂ and (26)₂ were simultaneously fitted to each dataset. The obtained model parameter values have been presented in Table 5, and Figs. 8 and 9 show the fitting results. The R^2 values possess their typical values with this model, in excess of 0.99.

The fitting results in Fig. 8 indicate the favourable correlation between the model predictions and the experimental data, with the relative errors below the typical 4% (except at the beginning of the deformation domain at small stretches). These results pertain to (extremely) soft hydrogels. The plots in Fig. 9, however, demonstrate the modelling results for tough(er) double-network hydrogel specimens.

Similar to the soft samples of Fig. 8, the fitting results in Fig. 9 indicate the capability of the model in capturing the finite deformation of (tough) double-network specimens. The relative errors are again around the

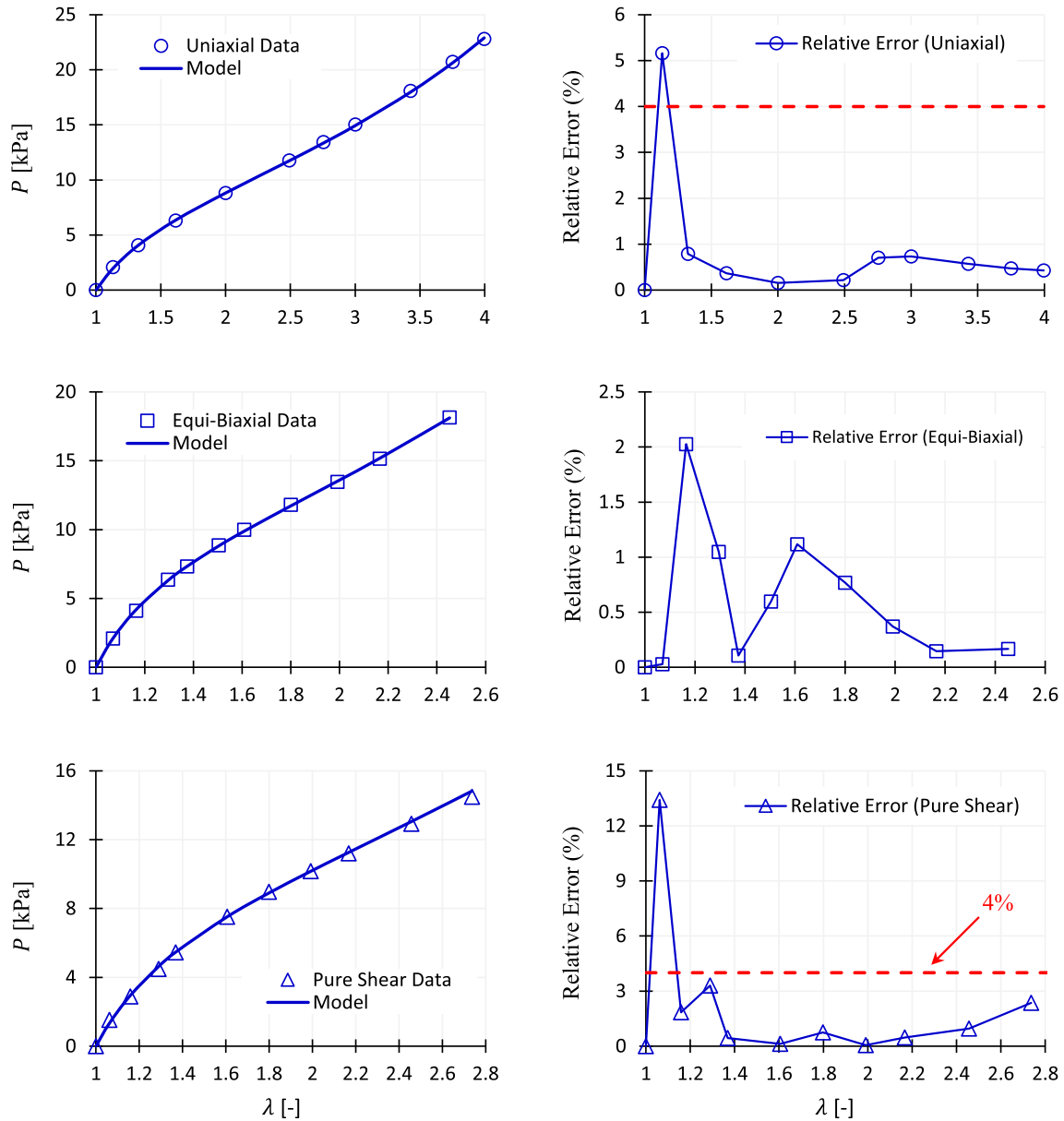


Fig. 8 Modelling results versus the experimental data due to Yohsuke et al. [26] for soft polyacrylamide (PAAm) hydrogel specimens under uniaxial, equi-biaxial and pure shear deformations. The panels on the right show the relative errors. The dotted (red) lines mark the error level at 4% (see the on-line version for plots in colour)

same typical level of 4%. We also note an interesting feature that the model appears to be capable of capturing, and that is the *continuous softening* in the loading curves. Unlike other hyperelastic models known to the author, which require to be augmented by a damage/softening variable, the proposed model here appears to be intrinsically able of capturing the softening via the inter-play between its constitutive parameters.

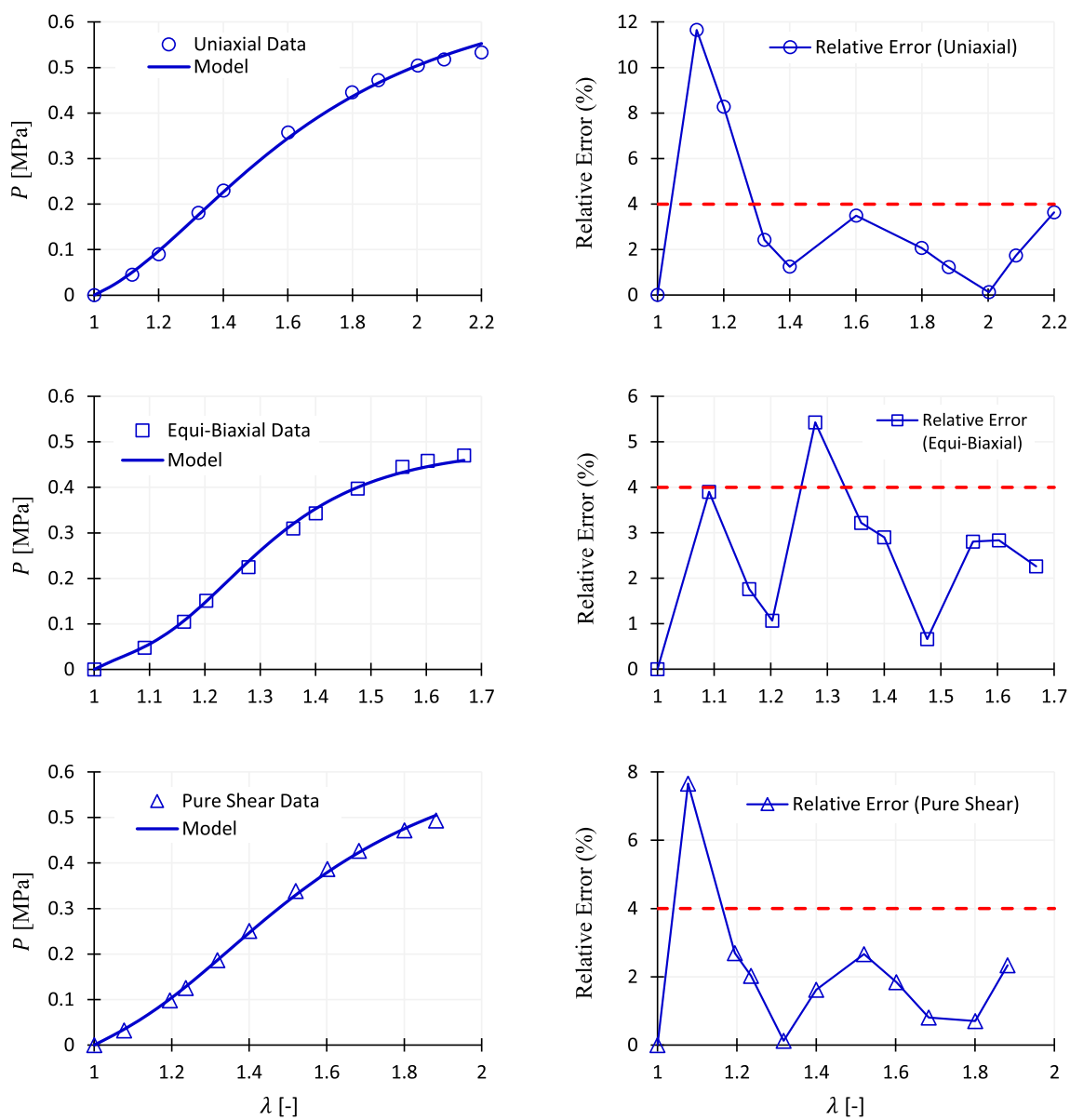


Fig. 9 Modelling results versus the experimental data due to Mai et al. [27] for double-network 'tough' hydrogel samples under uniaxial, equi-biaxial and pure shear deformations. The panels on the right show the relative errors. The dotted (red) lines mark the error level at 4% (see the on-line version for plots in colour)

Table 6 Model parameter values for the liquid crystal elastomer specimens due to Raistrick et al. [30], Merkel et al. [32] and (iii) Tokumoto et al. [31]

| | μ [kPa] | N [–] | n [–] | β [–] | C_2 [kPa] | ϵ [–] | R^2 |
|----------------------------|---------------------|---------|---------|-------------|--------------------|----------------|-------------------|
| Raistrick et al. [30] data | 0.105×10^3 | 54.19 | 19.69 | 3.90 | 7.78×10^3 | 0.29 | 0.99 ₉ |
| Merkel et al. [32] data | 0.195×10^3 | 3.17 | 1.53 | 0.72 | 1.00×10^3 | 0.08 | 0.99 ₉ |
| Tokumoto et al. [31] data | 7.28 | 0.93 | 0.48 | 1.11 | 226.62 | –0.45 | 0.99 ₆ |

3.3.5 Liquid crystal elastomers

The unique class of soft solids, called liquid crystal elastomers (LCEs), obtained by introducing liquid crystallinity into the elastomer polymeric networks [31, 56], exhibit an interesting set of mechanical behaviours. While some of the more nuanced aspects of those behaviours such as the rotation of nematic director and/or auxetic response etc. require a more comprehensive modelling approach; see, e.g. the contributions of Mihai and co-workers [29, 33], here we wish to correlate the datasets obtained from the uniaxial deformation of these elastomers with our proposed model in Eq. (3), only from the perspective of showcasing the suitability of the model to act as the hyperelastic base in those more advanced modelling frameworks to the finite deformation of LCEs.

In this regard, we consider three datasets on various LCE compounds under uniaxial deformation due to: (i) Raistrick et al. [30] with a monodomain nematic LCE specimen; (ii) Merkel et al. [32] with nematic-polymerised polydomain elastomers; and (iii) Tokumoto et al. [31] with a polydomain nematic elastomer exhibiting *soft elasticity*, i.e. a spontaneous deformation without (or with minimal) additional stress up to a certain stretch. The tabulated numerical data curated from these studies have been presented in Appendix A, Table 15. The relationship in Eq. (22) (i.e. the nominal stress) was fitted to the datasets of [30] and [32], while the Cauchy stress—deformation relationship in Eq. (21) was used for the dataset of [31]. The obtained model parameter values are given in Table 6, and the fitting results are illustrated in Fig. 10.

As the plots in Fig. 10 indicate, the model captures the basic uniaxial deformation behaviour of these LCE specimens favourably. The R^2 values are in excess of 0.99₆, and the relative errors for the first two datasets are below the typical 4%. For the dataset due to Tokumoto et al. [31], where the *soft elasticity* phenomenon occurs, the relative errors are higher. However, the model is capturing the phenomenon well, and is able to reproduce the trend rather accurately. There are no hyperelastic strain energy functions known to the author that have been shown to capture this behaviour in LCEs.

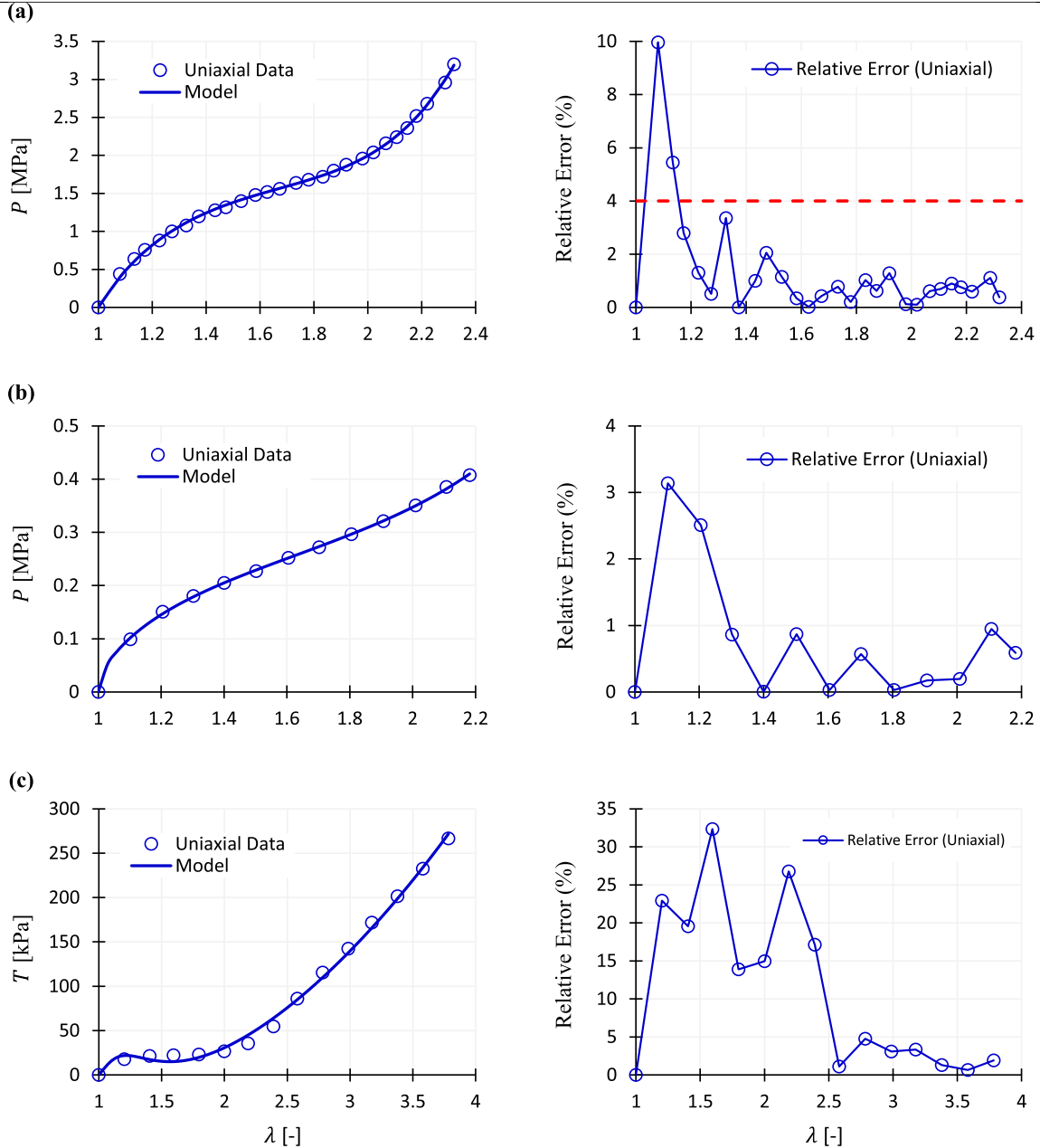


Fig. 10 Modelling results versus the experimental data for various liquid crystal elastomer samples under uniaxial tension due to: (a) Raistrick et al. [30]; (b) Merkel et al. [32]; and (c) Tokumoto et al. [31]. The panels on the right show the relative errors. The dotted (red) line marks the error level at 4%. Note that the stress measure in panel (c) is the Cauchy stress (see the on-line version for plots in colour)

3.3.6 Biomaterials

To present a well-rounded scope for application of the proposed model, we also consider some challenging datasets pertaining to the finite deformation of some biomaterial samples. These include the familiar dataset due to Budday et al. [34] on uniaxial tension and compression, and simple shear, deformations of the human brain tissue. The challenge in modelling this dataset is the highly nonlinear shear response, and the asymmetry of the tension—compression behaviour. Next we consider the uniaxial tension—compression of human whole blood clots due to Cahalane et al. [35], which again exhibits a distinctly asymmetric response. Finally, the simple shearing of a thrombus mimic specimen constructed from bovine blood due to Sugerman et al. [36] is considered. The challenging behaviour of this dataset is that the normal (to the sheared surface) stress

Table 7 Model parameter values for the human brain (cortex) tissue due Budday et al. [34]

| | μ [kPa] | N [–] | n [–] | β [–] | C_2 [kPa] | ϵ [–] | R^2 |
|-----------------|-------------|---------|-------------------|-------------|-------------|----------------|-------------------|
| Equi-biaxial | 26.63 | 53.24 | 0.96 ₅ | 7.74 | 1.16 | 11.48 | 0.99 ₈ |
| General biaxial | | | | | | | 0.99 ₂ |

Table 8 Model parameter values for the human blood clot and thrombus mimic samples due to Cahalane et al. [35] and Sugerman et al. [36], respectively

| | Cahalane et al. data [35] | | | | | | |
|----------------------------------|---------------------------|---------|---------|-------------|-------------|----------------|-------------------|
| | μ [kPa] | N [–] | n [–] | β [–] | C_2 [kPa] | ϵ [–] | R^2 |
| Uniaxial tension and compression | 10.37 | – 1.74 | 9.92 | 0.89 | 100.05 | – 0.06 | 0.99 ₈ |
| | Sugerman et al. data [36] | | | | | | |
| | μ [kPa] | N [–] | n [–] | β [–] | C_2 [kPa] | ϵ [–] | R^2 |
| Simple shear | 5.61 | 99.95 | 1.11 | 2.42 | 7.03 | – 0.25 | 0.99 |
| Normal stress (P_{22}) | | | | | | | 0.87 |

component of simple shear deformation shows the unusual *reverse* Poynting effect. These datasets provide a reasonable basis to test the ability of the model for biomaterials applications too.

Accordingly, Eqs. (22) and (29)₁ were simultaneously fitted to the dataset of [34], while for [35] only Eq. (22) was used. However, for applying the model to the dataset from [36], we must first derive the ensuing relationship for the normal stress T_{22} under simple shear using [53]:

$$T_{22} = -2\gamma^2 W_2, \quad (30)$$

which, on using Eq. (3), yields:

$$T_{22} = -\frac{2}{3^\epsilon} C_2 \epsilon \gamma^2 I_2^{\epsilon-1}, \quad (31)$$

where I_2 has been defined just after Eq. (29). The equivalent nominal stress P_{22} is obtained via: $P_{22} = T_{22}/\lambda_2$, where we note that $\lambda_2 = -\frac{\gamma}{2} + \sqrt{1 + \frac{\gamma^2}{4}}$, as:

$$P_{22} = -\frac{2}{3^\epsilon} C_2 \epsilon \frac{\gamma^2}{-\frac{\gamma}{2} + \sqrt{1 + \frac{\gamma^2}{4}}} I_2^{\epsilon-1}. \quad (32)$$

The relationships in Eqs. (29)₁ and (32) were subsequently fitted to the dataset of Sugerman et al. [36]. The tabulated datapoints of [34] has been presented elsewhere [14], and those for [35] and [36] are given in Appendix A, Tables 16 and 17, respectively.

Starting with human brain dataset [34], the identified model parameters are listed in Table 7, and the plots in Fig. 11 demonstrate the modelling results. The R^2 values are in excess of 0.99, and the model captures both the asymmetry of the compression—tension and nonlinearity of the shear response well. While the resulting relative errors are above the typical 4% of the preceding datasets, we note that challenging nature of this particular dataset, and the even higher relative errors provided by other ‘gold-standard’ models in the literature. By way of comparison, we reproduce here from [15] the relative error plots for the same dataset using the three-term Ogden model; see Fig. 11c. It is observed that the proposed model provides improved fits.

The modelling results for the human (whole) blood clot and thrombus mimic specimens are presented in Fig. 12. Table 8 summarises the model parameter values. The model is seen to capture the distinct asymmetry of the compression—tension deformation of whole blood clot favourably, with the R^2 value in excess of 0.99₈ and the relative errors typically below 8% (except for small levels of compression). For the thrombus mimic specimen (from bovine blood), the model captures well the simple shear behaviour, and also correctly predicts the *reverse* Poynting effect (the P_{22} component of the stress in simple shear). However, the quality of the fits, particularly in the case of latter, can be improved. One way of achieving this improvement is to perhaps opt for another functional form of the I_2 term in Eq. (8), seeing that only the response function W_2 appears in T_{22} or

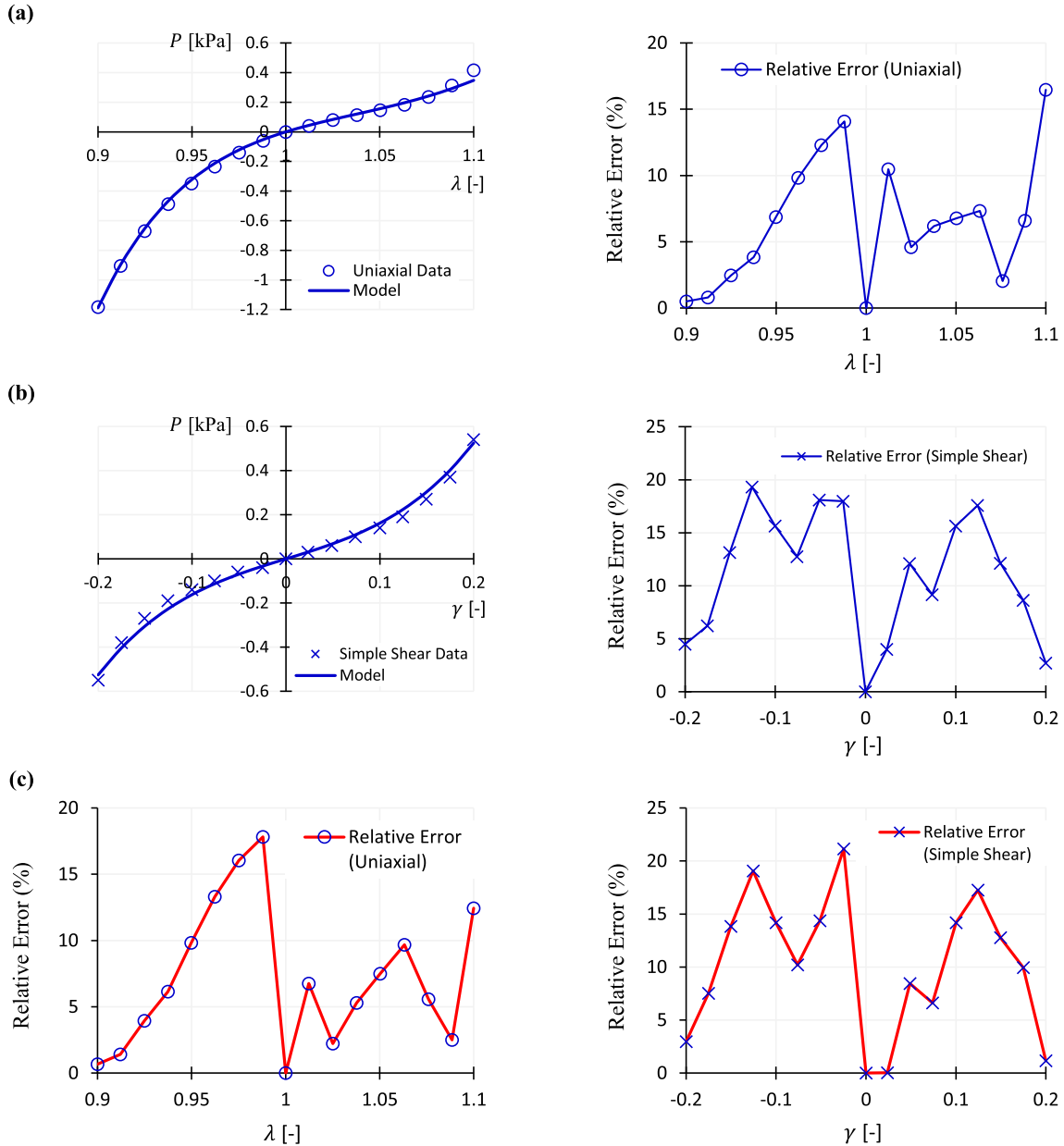


Fig. 11 Modelling results versus the experimental data for the human brain (cortex) tissue due Budday et al. [34]: **a** Uniaxial compression – tension; **b** Simple shear; **c** The relative errors using the 3-term Ogden model for the same dataset (left panel: uniaxial deformation data; right panel: simple shear data), reproduced from [15] (see the on-line version for plots in colour)

P_{22} relationships in Eqs. (31) or (32), respectively. However, this premise will not be pursued here. Our main aim here is to demonstrate that such a relatively simple functional form of the model in Eq. (3) is capable of capturing a wide range of datasets and challenging deformation behaviours, with a very good accuracy. For particular datasets/specimens, such as that of the thrombus mimic specimen [36], the proposed framework here offers the flexibility for choosing specific $W(I_2)$ functions to get better fits, on an empirical basis, if required.

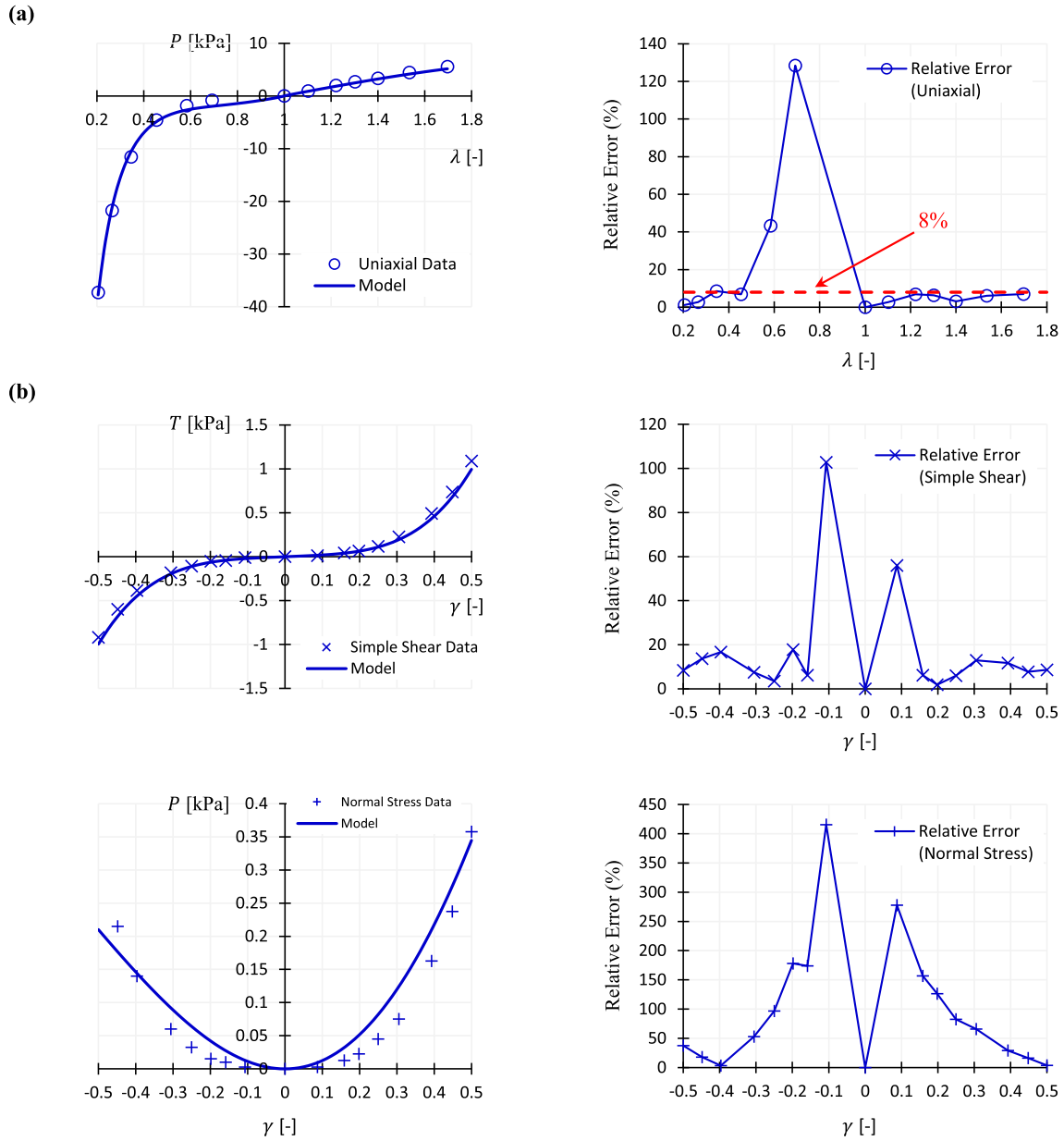


Fig. 12 Modelling results versus the experimental data for: **a** human (whole) blood clot under uniaxial compression – tension, due to Cahalane et al. [35]; and **b** thrombus mimic specimen constructed from bovine blood under simple shear and measuring the normal component of the stress, due to Sugerman et al. [36]. The panels on the right show the relative errors. The dotted (red) line marks the error level at 8% (see the on-line version for plots in colour)

4 Some points of discussion

The application of the proposed model in Eq. (3) to a wide range of soft materials and deformation modes was presented in the previous section. The correlation between the model and the data was seen to be favourable, and many challenging aspects of the finite deformation of the various considered specimens were captured by the model. However, there are some more-nuanced modelling aspects which may prove worthy of further analysis. Those will be discussed in the following.

4.1 Model predictions

It appears a tempting prospect to have, and use, a model to *predict* the mechanical behaviour of a subject material *a priori*, as opposed to *a posteriori* simulating that behaviour via fitting the model to the dataset first. Microstructural-based models can certainly hope to enable such predictions, to the extent that their constitutive parameters can be independently (of mechanical deformation data) obtained and plugged into the model, so that they can then truly predict the mechanical response of the material under a given boundary value problem. Until that hope is realised, due care and attention must be afforded to exercises in which by fitting a model to a dataset one asserts to be able to predict another deformation behaviour of the same specimen. Such an exercise, and assertion, is fraught with mathematical and mechanical inconsistencies.

First, numerical examples exist in the literature which clearly show that the global minimum of the minimisation objective function (e.g. the RSS function in our case) is not necessarily achieved on using one deformation dataset, and instead is more likely achieved when multiaxial deformation datasets are used in simultaneous fittings; see, e.g. Appendix B of [50]. Therefore, if a model is fitted only to one deformation dataset, the obtained model parameter values may not necessarily be the global values of the constitutive parameters of the material. By luck, and due to potential collinearities in the data [54, 55], a model calibrated that way may ‘predict’ another deformation; however, such an event will not be reproducible and/or repeatable. This problem is further exacerbated by the increase in number of model parameters, as discussed at length by Ogden et al. [19], in which case even finding a unique optimum fit (and thereby the optimum model parameter values) is not guaranteed.

Second, and perhaps more importantly, is the problem astutely noted by Holzapfel and Ogden [57]. Their focus there is on anisotropic models; however, the same notion is also applicable to the isotropic case. Therein they discuss that by fitting a model to a dataset, one is essentially trying to solve for, and characterise, the response function of the model through finding the model parameters via the process of minimisation (i.e. fitting). If, then, the model has one response function, one set of deformation data should suffice for this characterisation. If a model has two response functions, then two sets of independent deformation datasets are required, and so on. Therefore, if a model has only one response function, and its mathematical form is such that the optimal model parameter values can be identified by a single fit, it is only then that one can hope for being able to *predict* another deformation behaviour by the model.

Consequently, for a model such as that proposed in Eq. (3), where two response functions W_1 and W_2 are present, it needs to be calibrated by *at least* two independent deformation datasets, before it can be used for *predicting* other behaviours of the same material. Accordingly, in this section we demonstrate the *predictive* capability of our proposed model, when calibrated with the required number of datasets. As a starting point, we consider the canonical Treloar dataset [20], where we first calibrate the model with the equi-biaxial and pure shear datasets, by simultaneous fits using Eqs. (23)₂ and (26)₂, and subsequently *predict* the uniaxial behaviour with the so identified model parameters, using Eq. (22). The result is shown in Fig. 13. It is observed that the *predicted* uniaxial behaviour correlates favourably with the data.

Next, we consider *predicting* an additional behaviour of a specimen using the simultaneous multiaxial fit carried out in Sect. 3. To this end, we consider the rubber vulcanisate specimens due to Kawabata et al. [21], where using the identified model parameters in Table 1, obtained by simultaneous fitting of the model to uniaxial, equi-biaxial and pure shear deformations, we *predict* the lateral stress—deformation curve in pure shear. It may be informative to note that the lateral component of the Cauchy stress in pure shear, $(T_{22})_{ps}$, for the proposed model in Eq. (3) is related to the principal stretch λ as:

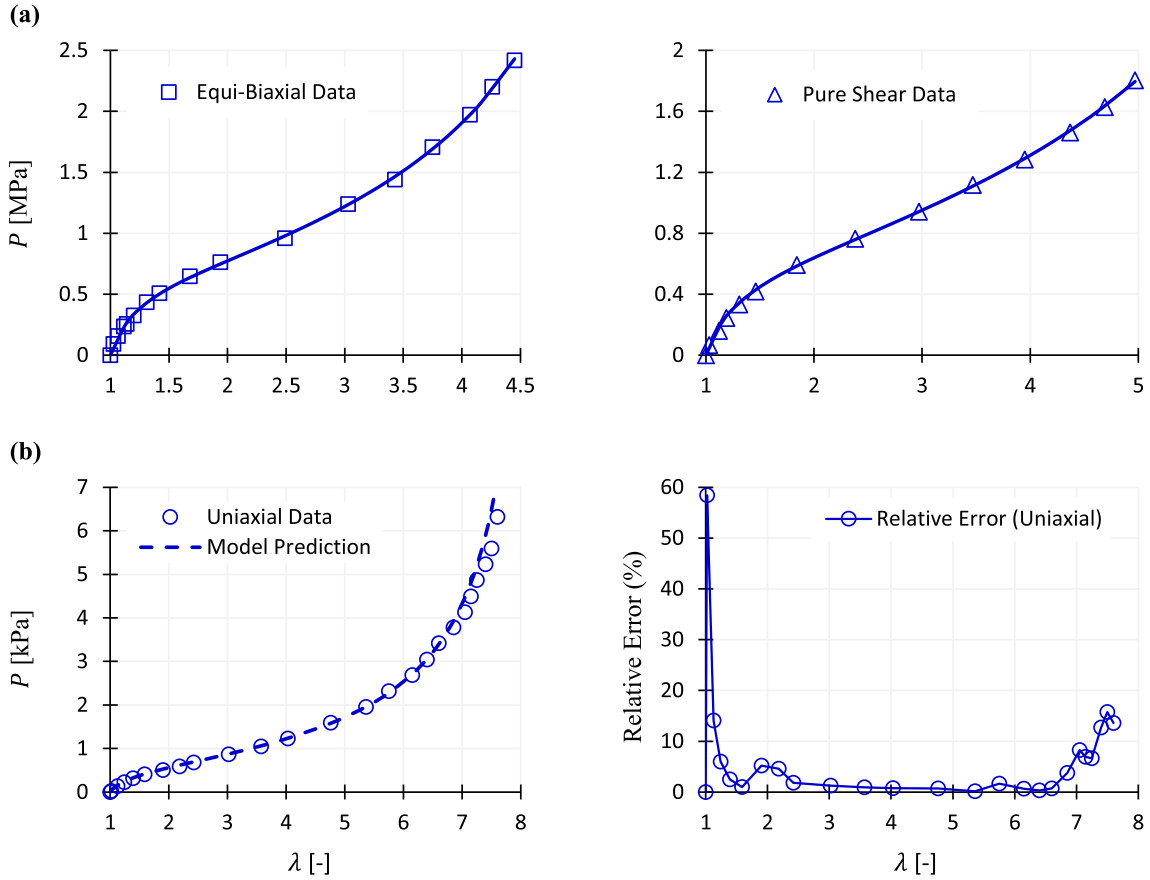


Fig. 13 Predicting the uniaxial deformation behaviour of Treloar's dataset [20] by first fitting the model to equi-biaxial and pure shear deformations: **a** fitting results; and **b** prediction of the uniaxial deformation versus the experimental data. The calibrated model parameters are: $\mu = 0.37$ [MPa], $N = 24.33$ [-], $n = 2.71$ [-], $\beta = 0.795$ [-], $C_2 = 0.24$ [MPa], and $\epsilon = 0.45$ [-]. The R^2 value for the predicted uniaxial behaviour is 0.98

$$(T_{22})_{ps} = \frac{\mu\beta}{n} \frac{I_1(I_1 - 3)^{\beta-1} + 3N[1 - (I_1 - 3)^{\beta-1}] - 3nN \left(1 - \frac{1}{\lambda^2}\right) + \frac{2C_2\epsilon}{3\epsilon} I_2^{\epsilon-1}(\lambda^2 - 1)}{I_1 - 3N}. \quad (33)$$

Since in pure shear $\lambda_2 = 1$, we find that the nominal stress $(P_{22})_{ps}$ —stretch λ relationship is also identical to that of Eq. (33). The *prediction* results using Eq. (33) and the model parameter values in Table 1 are compared against the experimental data of Kawabata et al. [21] in Fig. 14. The affinity between the model predictions and the data is clear from the plot.

As a further example, here we present another *prediction* of the lateral stress $(P_{22})_{ps}$ —stretch λ behaviour under pure shear deformation of the soft polyacrylamide (PAAm) hydrogel specimens due to Yohsuke et al. [26]. This *prediction* has been obtained on using Eq. (33) and the identified parameter values listed in Table 5 (which were attained via the simultaneous fit of the model to uniaxial, equi-biaxial and pure shear deformations). The prediction results are illustrated in Fig. 15. It is again observed that the model *predicts* the data favourably, with the value of R^2 in excess of 0.985.

Finally, here we present the model *predictions* of the general biaxial behaviour of the double-network ‘tough’ hydrogel samples due to Mai et al. [27]. In Sect. 3 we presented the identified model parameters on simultaneous fitting of the model to the uniaxial, equi-biaxial and pure shear deformation datasets—see Table 5. Using those values, and the relationships in Eq. (25), the behaviour of the specimens under a general biaxial deformation was *predicted*. The plots in Fig. 16 compare the model predictions versus the experimental data. The model is again observed to predict the data favourably, with R^2 values in excess of 0.99.

We conclude that subject to it being calibrated appropriately, the proposed model in Eq. (3) is well capable of *predicting* the other deformation behaviours of soft materials, exemplified here for various deformations

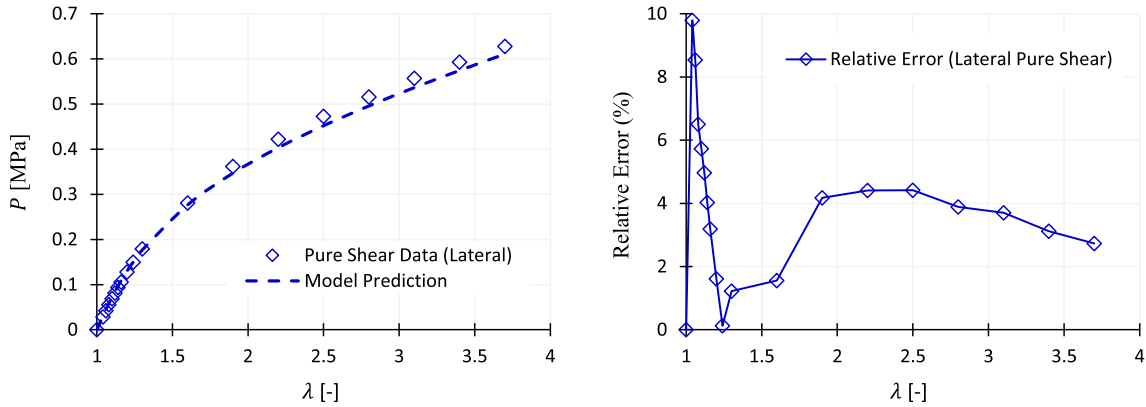


Fig. 14 Predicting the lateral behaviour under pure shear deformation of the isoprene rubber vulcanisate specimens due to Kawabata et al. [21]. Model predictions have been generated on using Eq. (33) and the model parameter values in Table 1. The R^2 value for the predicted behaviour is 0.997

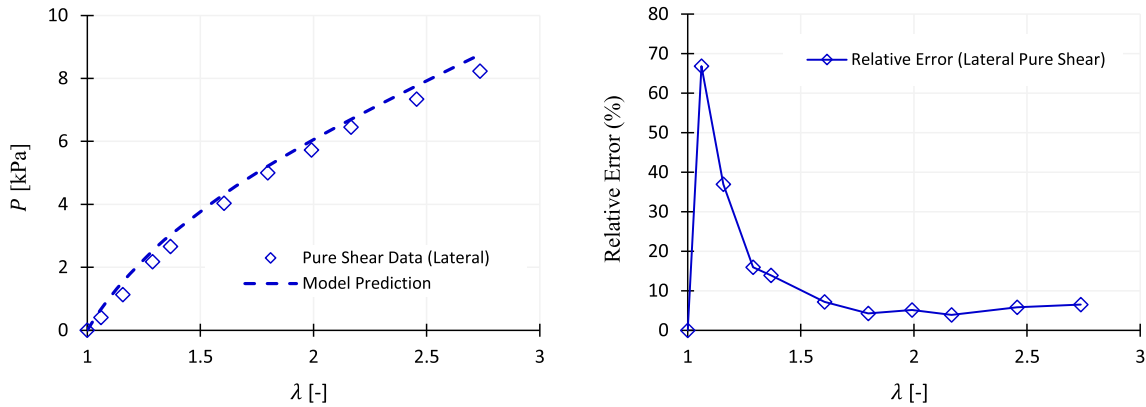


Fig. 15 Predicting the lateral behaviour under pure shear deformation of PAAm hydrogel specimens due to Yohsuke et al. [26]. Model predictions have been generated on using Eq. (33) and the model parameter values in Table 5. The R^2 value for the predicted behaviour is 0.985

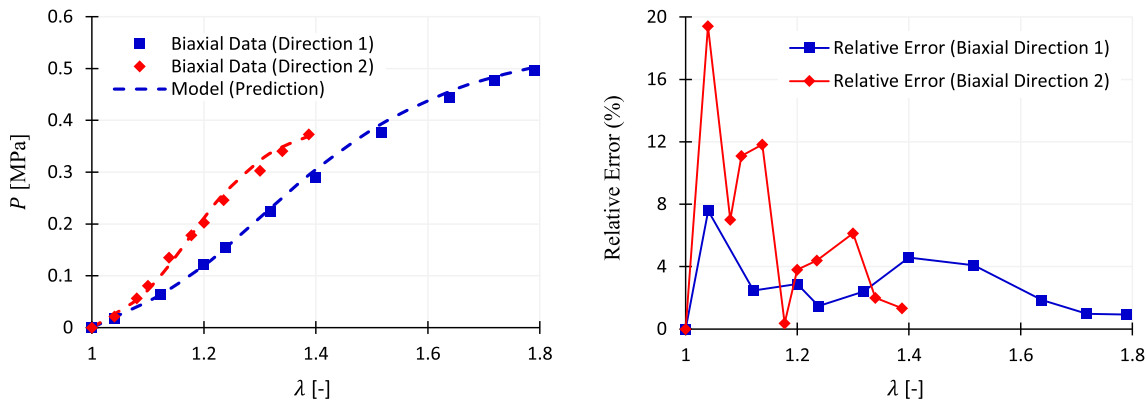


Fig. 16 Predicting the general biaxial behaviour of the double-network hydrogel samples due to Mai et al. [27]. Model predictions have been generated on using Eq. (25) and the model parameter values in Table 5. The R^2 values for the predicted behaviours are in excess is 0.99 (see the on-line version for plots in colour)

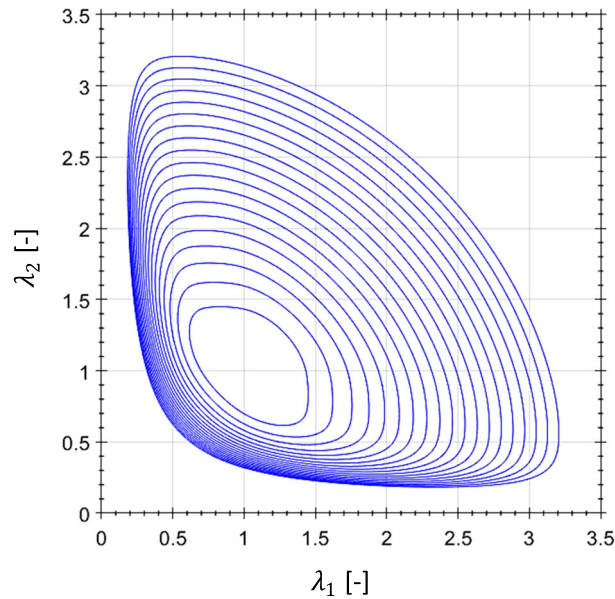


Fig. 17 The iso-energy plots in (λ_1, λ_2) plane using the identified parameter values for the hydrogel specimens of Mai et al. [27] in Table 5. The plots verify the convexity of the strain energy function

modes including uniaxial, general biaxial and pure shear deformations, on using the canonical datasets of Treloar [20] and Kawabata et al. [21], and for various elastomers such as hydrogels [26, 27].

4.2 Issues surrounding the empirical inequalities and convexity

Of the datasets modelled in this work, we note those of [25, 27] and [35], for which the identified values of model parameter N (and also n in the case of [25]) were negative. Following *Remark 2*, it can be easily verified that such values do not result in an unphysical consequence or behaviour. For example, the ensuing values of the infinitesimal shear modulus μ_0 given by Eq. (9) using the values listed in Tables 3, 5 and 8 for the specimens of [25, 27] and [35], are 363.34 kPa, 0.04 MPa and 1.49 kPa, respectively. As a case in point, we also present the iso-energy plots of the resulting W function of Eq. (3) using the identified model parameter values in Table 5 for hydrogel specimen of [27]. These are shown in Fig. 17, and verify the convexity of the iso-energy plots.

Similarly, we note the datasets of [25, 27, 31, 35] and [36], for which the identified value of ε is negative. In view of *Remark 1*, for those datasets, the empirical relationship $W_2 \geq 0$ is not satisfied. For the three datasets [25, 27] and [35], as was discussed in the foregoing, no unphysical consequences arise. It can be verified that the other two datasets, namely those of [31] and [36], do not report unphysical values for the infinitesimal shear modulus either, with the values of μ_0 being 47.52 kPa and 0.175 kPa, respectively. As regards to convexity, Fig. 18 presents the iso-energy plots of the ensuing strain energy function W for these two datasets, using the identified model parameter values in Tables 6 and 8. For the Sugerma et al. data [36], the convexity of the iso-energy plots is evident (Fig. 18a). This further reinforces the point made in *Remark 1*, that by allowing $\varepsilon \in \mathbb{R}$ rather than restricting it to \mathbb{R}^+ space, features such as the *reverse* Poynting effect can be captured without inflicting any unwanted ill-posed effects. However, for the Tokumoto et al. [31], the iso-energy plots are only piece-wise convex (Fig. 18b). This is expected though, since a consequence of lack of convexity is the loss of one-to-one correspondence between the deformation and stress pairs (see, e.g. [58]). As the experimental data and modelling results for this dataset indicate—see Fig. 10c, this one-to-one correspondence is clearly lost within the domain of deformation, where the *soft elasticity* phenomenon occurs. Therefore, the ensuing strain energy function would have been expected to lose convexity in this domain. The modelling results hence appear to be consistent.

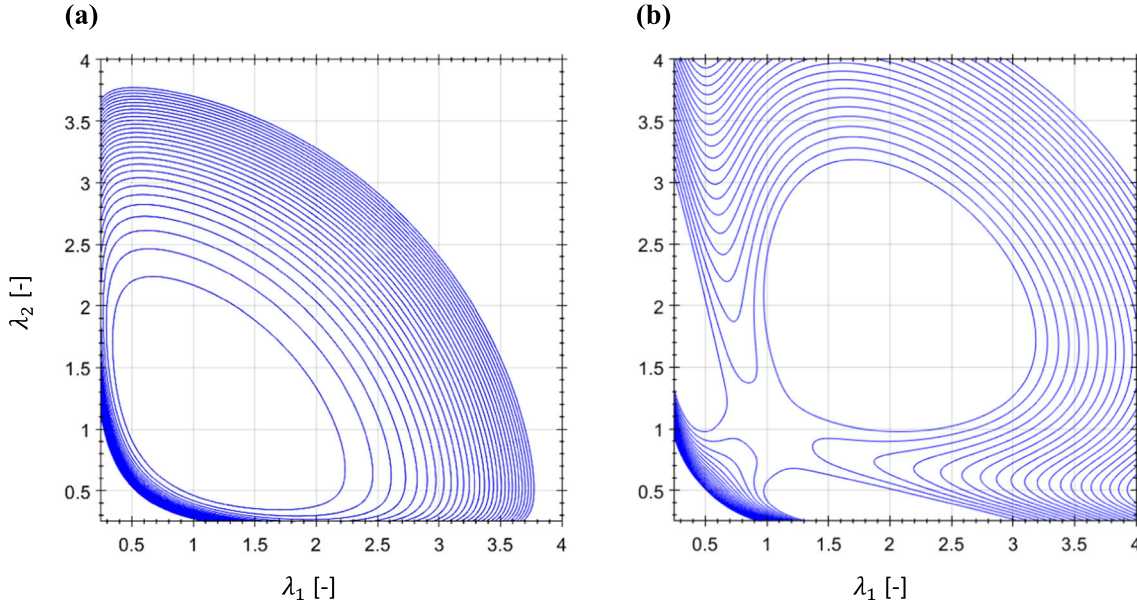


Fig. 18 The iso-energy plots in (λ_1, λ_2) plane for: **a** thrombus mimic due to Sugerman et al. [36]; and **b** LCE specimen of Tokumoto et al. [31]

4.3 A further generalisation of the model

It is possible to achieve more generalised functional forms of the model in Eq. (3) on using other I_2 functions than that used in Eq. (8). An ad hoc example, inspired by the functional form of the $W(I_1)$ part of the model in Eq. (7) may be:

$$W(I_2) = \frac{3(m-1)}{m} C_2 \left\{ \frac{1}{3(m-1)} \left[\left(\frac{I_2}{3} \right)^\epsilon - 1 \right] + \ln \left(\frac{I_2}{3} \right)^\epsilon \right\}, \quad (34)$$

subject to the same conditions on the parameters: $m, C_2 \in \mathbb{R}^+$; $\epsilon \in \mathbb{R}$. The adjunct I_2 -term in Eq. (34) helps the ensuing $W(I_1, I_2)$ model to be *parent* to additional models (in addition to all the invariants-based models recounted in Sect. 2; just before Sect. 3), such as that of Pucci and Saccomandi [39] and the Gent-Thomas model [59]. Note that:

$$\lim_{m \rightarrow \infty} W(I_2) = 3C_2 \epsilon \ln \left(\frac{I_2}{3} \right), \quad (35)$$

which, on considering $3C_2\epsilon \equiv C_2$, is the I_2 -term in those models. However, with the extra model parameter that such generalisation introduces compared with the model in Eq. (3), no noticeable (if any) improvement was observed in the quality of fits to the considered datasets here. Therefore, from a modelling perspective, there may not be much point, or advantage, on pursuing further invariants-based generalisation of the model in Eq. (3); except that from a mathematical point of view a more universal model may be obtained.

Another adjustment may be to consider a variant of the $W(I_1)$ function in Eq. (7), in the form:

$$W(I_1) = \frac{3(n-1)}{2n} \mu N \left[\frac{1}{3N(n-1)} (I_1^\beta - 3^\beta) - \ln \left(\frac{I_1 - 3N}{3 - 3N} \right)^\beta \right]. \quad (36)$$

It can be verified that at the limit $n \rightarrow 1$, the multi-term functional form of Eq. (36) reduces to:

$$\lim_{n \rightarrow \infty} W(I_1) = \sum_i \frac{1}{2} \mu_i \left(I_1^{\beta_i} - 3^{\beta_i} \right), \quad (37)$$

which is akin to the model by Lopez–Pamies [48], and for when $\beta_i \in \mathbb{N}$ is akin to the Arruda–Boyce [60] model. However, we note that the functional form in Eq. (36) then will not be a direct parent to polynomial forms of

the neo-Hookean function such as that of Yeoh's cubic model [46]. Therefore, this functional form does not offer an advantage over that of Eq. (7) considered in this study, in terms of providing a more comprehensive universality. We did not also find a discernible difference between the quality of fits when incorporating this functional form into the model, versus those provided here.

5 Concluding remarks

A generalised $W(I_1, I_2)$ strain energy function of binomial form was presented in this work for application to the finite deformation of isotropic incompressible soft solids. The model is a generalisation of a previously devised model that has a [1/1] rational response function [13] in I_1 , to the current general [$\beta/1$] order, and the generalisation of the Carroll-type I_2 function [44] to a general power ϵ . The ensuing model with six parameters, Eq. (3), was then applied to the multiaxial deformation of a wide range of materials, from filled and unfilled rubbers to hydrogels, liquid crystal elastomers and biomaterials. It was shown that the model captures the experimental data accurately, with typical relative errors of below 4% in the engineering space. Various challenging modelling aspects such as the asymmetry of compression—tension, high nonlinearity of the simple shear response, deformation softening effects, pronounced Payne effect, the *soft elasticity* phenomenon, and the *reverse* Poynting effect, were demonstrated to be favourably captured by the model. When calibrated appropriately, the model *predictions* were shown to closely match the experimental data too. It was further shown that the proposed model here is the *parent* to many of the well-known existing invariants-based models in the literature. There are very few, if any, models in the current literature that embody these features with relatively low number of model parameters, and are capable of such width and depth of application. Given the analyses and results presented here, the devised model is proposed as a standard choice for *a priori* selection for application to the finite deformation of isotropic incompressible soft materials. Further generalisation of the model may be achieved by enhancing the functional form of the current model using the principal stretches λ_i , and will be investigated in a future work.

Data availability The data used in this manuscript have either been presented in authors' preceding works (e.g. [13, 15, 16, 50]), as cited in the text, or presented in Appendix A, Tables 9, 10, 11, 12, 13, 14, 15, 16 and 17.

Declarations

Conflict of interest The author declares no conflict of interest.

Open Access This article is licensed under a Creative Commons Attribution 4.0 International License, which permits use, sharing, adaptation, distribution and reproduction in any medium or format, as long as you give appropriate credit to the original author(s) and the source, provide a link to the Creative Commons licence, and indicate if changes were made. The images or other third party material in this article are included in the article's Creative Commons licence, unless indicated otherwise in a credit line to the material. If material is not included in the article's Creative Commons licence and your intended use is not permitted by statutory regulation or exceeds the permitted use, you will need to obtain permission directly from the copyright holder. To view a copy of this licence, visit <http://creativecommons.org/licenses/by/4.0/>.

Appendix A: Tabulated numerical data for some of the datasets used in this study

See Tables 9, 10, 11, 12, 13, 14, 15, 16 and 17.

Table 9 Tabulated numerical datapoints collated from Hohenberger et al. [23]

| λ [-] | P [MPa] |
|-------------------|---------------------|
| 0.71 | - 7.37 ₅ |
| 0.75 | - 6.37 ₅ |
| 0.81 | - 5.00 |
| 0.87 | - 3.75 |
| 0.91 | - 2.87 ₅ |
| 0.95 | - 1.81 |
| 0.98 ₅ | - 0.75 |
| 1.00 | 0 |
| 1.02 | 1.01 ₅ |
| 1.06 | 2.09 ₅ |
| 1.10 | 2.98 |
| 1.17 ₅ | 3.55 ₅ |
| 1.26 | 4.13 |
| 1.37 ₅ | 4.76 |
| 1.46 | 5.21 |
| 1.58 | 5.97 |
| 1.70 | 6.73 |
| 1.82 | 7.55 ₅ |
| 1.94 | 8.44 |
| 2.10 | 9.75 |

Table 10 Tabulated numerical datapoints collated from Lahellec et al. [22]

| Uniaxial | | Simple shear | |
|-------------------|-------------------|-------------------|-------------------|
| λ [-] | P_{uni} [MPa] | γ [-] | P_{ss} [MPa] |
| 1.00 | 0 | 0 | 0 |
| 1.01 | 0.14 | 0.02 | 0.07 |
| 1.04 | 0.43 | 0.04 | 0.15 |
| 1.07 ₅ | 0.70 | 0.07 | 0.27 |
| 1.11 | 0.88 | 0.11 | 0.37 |
| 1.15 | 1.04 | 0.14 | 0.44 |
| 1.19 | 1.19 | 0.18 | 0.50 |
| 1.23 | 1.33 | 0.21 | 0.55 |
| 1.26 | 1.46 | 0.25 | 0.61 |
| 1.30 | 1.58 ₅ | 0.29 | 0.66 |
| 1.34 | 1.70 ₅ | 0.32 | 0.72 |
| 1.38 | 1.81 | 0.36 | 0.78 |
| 1.42 | 1.91 | 0.39 | 0.84 |
| 1.45 | 2.01 | 0.43 | 0.89 ₅ |
| 1.49 | 2.11 | 0.46 | 0.95 |
| 1.53 | 2.22 | 0.50 | 1.01 |
| 1.57 | 2.33 ₅ | 0.53 ₅ | 1.06 |
| 1.60 | 2.46 | 0.57 | 1.11 ₅ |
| 1.64 | 2.59 | 0.61 | 1.17 |
| | | 0.64 | 1.21 |

Table 11 Tabulated numerical datapoints collated from Meunier et al. [24]

| Uniaxial | | Equi-biaxial | | Pure shear | |
|-------------------|---------------------|-------------------|-------------------|-------------------|-------------------|
| λ [-] | P_{uni} [MPa] | λ [-] | P_{eq-bi} [MPa] | λ [-] | P_{ps} [MPa] |
| 0.39 | - 2.39 | 1.00 | 0 | 1.00 | 0 |
| 0.45 | - 1.64 | 1.04 ₅ | 0.10 ₅ | 1.01 | 0.04 |
| 0.52 | - 1.18 ₅ | 1.10 | 0.18 | 1.04 ₅ | 0.10 |
| 0.61 | - 0.80 | 1.18 | 0.28 | 1.09 | 0.14 |
| 0.66 | - 0.58 ₅ | 1.23 ₅ | 0.33 | 1.15 | 0.19 |
| 0.72 | - 0.42 | 1.34 | 0.41 | 1.21 | 0.24 ₅ |
| 0.78 | - 0.29 | 1.44 ₅ | 0.48 | 1.29 | 0.30 |
| 0.85 | - 0.18 | 1.54 | 0.54 | 1.38 | 0.35 |
| 0.91 | - 0.09 ₅ | 1.68 | 0.65 | 1.48 | 0.40 |
| 0.95 ₅ | - 0.04 | 1.78 | 0.74 | 1.57 | 0.45 |
| 1.00 | 0 | 1.81 | 0.77 | 1.67 | 0.50 |
| 1.05 | 0.04 | 1.85 | 0.82 | 1.76 | 0.55 |
| 1.11 | 0.10 | 1.96 | 1.01 | 1.84 ₅ | 0.60 |
| 1.18 | 0.14 | 2.07 | 1.32 | 1.92 | 0.65 |
| 1.26 ₅ | 0.20 | | | 1.98 | 0.70 |
| 1.36 | 0.24 ₅ | | | 2.03 | 0.75 |
| 1.46 | 0.30 | | | 2.09 | 0.80 |
| 1.56 | 0.35 | | | | |
| 1.66 ₅ | 0.40 | | | | |
| 1.76 | 0.45 | | | | |
| 1.85 | 0.50 | | | | |
| 1.93 | 0.55 | | | | |
| 2.04 | 0.65 | | | | |
| 2.09 | 0.70 | | | | |

Table 12 Tabulated numerical datapoints collated from Jiang et al. [25]

| Equi-biaxial | | | General biaxial | | |
|-------------------|---------------------|-------------------|---------------------|-----------------|---------------------|
| λ [-] | P_{eq-bi} [kPa] | λ_1 [-] | $(P_{bi})_1$ [kPa] | λ_2 [-] | $(P_{bi})_2$ [kPa] |
| 1.00 | 0 | 1.00 | 0 | 1.00 | 0 |
| 1.03 | 62.38 | 1.03 | 62.74 | 1.03 | 55.73 |
| 1.08 | 120.97 ₅ | 1.05 | 95.95 | 1.08 | 116.68 ₅ |
| 1.13 | 176.74 | 1.07 | 125.48 | 1.12 | 171.42 |
| 1.18 ₅ | 232.50 | 1.08 ₅ | 147.62 | 1.18 | 224.40 ₅ |
| 1.23 | 268.41 ₅ | 1.11 | 172.61 | 1.25 | 282.13 ₅ |
| 1.29 | 313.78 | 1.13 | 195.60 | 1.31 | 322.19 |
| 1.34 | 351.589 | 1.15 | 223.27 | 1.37 | 362.25 |
| 1.39 | 387.50 | 1.19 | 258.33 | 1.42 | 398.82 |
| 1.45 | 430.98 | 1.22 | 284.01 | 1.46 | 431.91 |
| 1.50 | 472.56 | 1.25 | 305.15 ₅ | 1.50 | 459.78 |

Table 13 Tabulated numerical datapoints collated from Yohsuke et al. [26]

| Uniaxial | | Equi-biaxial | | Pure shear | |
|---------------|-----------------|-------------------|--------------------|-------------------|----------------|
| λ [-] | P_{uni} [kPa] | λ [-] | P_{eq-bi} [kPa] | λ [-] | P_{ps} [kPa] |
| 1.00 | 0 | 1.00 | 0 | 1.00 | 0 |
| 1.13 | 2.08 | 1.07 | 2.10 | 1.06 | 1.52 |
| 1.32 | 4.08 | 1.16 ₅ | 4.11 | 1.16 | 2.88 |
| 1.61 | 6.32 | 1.30 | 6.37 | 1.29 | 4.48 |
| 2.00 | 8.80 | 1.37 | 7.34 | 1.37 | 5.44 |
| 2.49 | 11.76 | 1.50 | 8.87 | 1.60 ₅ | 7.52 |
| 2.75 | 13.44 | 1.61 | 10.00 | 1.80 | 8.96 |
| 3.00 | 15.04 | 1.80 | 11.81 | 1.99 | 10.16 |
| 3.43 | 18.08 | 1.99 | 13.47 | 2.17 | 11.20 |
| 3.75 | 20.72 | 2.16 ₅ | 15.16 | 2.46 | 12.92 |
| 4.00 | 22.80 | 2.45 | 18.14 ₅ | 2.74 | 14.48 |

Table 14 Tabulated numerical datapoints collated from Mai et al. [27]

| Uniaxial | | Equi-biaxial | | Pure shear | |
|---------------|-------------------|---------------|-------------------|-------------------|-------------------|
| λ [-] | P_{uni} [kPa] | λ [-] | P_{eq-bi} [kPa] | λ [-] | P_{ps} [kPa] |
| 1.00 | 0 | 1.00 | 0 | 1.00 | 0 |
| 1.12 | 0.04 ₅ | 1.09 | 0.05 | 1.08 | 0.03 |
| 1.20 | 0.09 | 1.16 | 0.10 ₅ | 1.19 ₅ | 0.10 |
| 1.32 | 0.18 | 1.20 | 0.15 | 1.24 | 0.12 ₅ |
| 1.40 | 0.23 | 1.28 | 0.22 ₅ | 1.32 | 0.19 |
| 1.60 | 0.36 | 1.36 | 0.31 | 1.40 | 0.25 |
| 1.80 | 0.44 ₅ | 1.40 | 0.34 | 1.52 | 0.34 |
| 1.88 | 0.47 | 1.48 | 0.40 | 1.60 | 0.39 |
| 2.00 | 0.50 | 1.56 | 0.44 ₅ | 1.68 | 0.43 |
| 2.08 | 0.52 | 1.60 | 0.46 | 1.80 | 0.47 |
| 2.20 | 0.53 | 1.67 | 0.47 | 1.88 | 0.49 |

Table 15 Tabulated numerical datapoints for liquid crystal elastomers

| Raistrick et al. data [30] | | Merkel et al. data [32] | | Tokumoto et al. data [31] | |
|----------------------------|-----------------|-------------------------|-------------------|---------------------------|---------------------|
| λ [-] | P_{uni} [MPa] | λ [-] | P_{uni} [MPa] | λ [-] | T_{uni} [kPa] |
| 1.00 | 0 | 1.00 | 0 | 1.00 | 0 |
| 1.08 | 0.44 | 1.10 | 0.10 | 1.20 | 17.78 |
| 1.13 | 0.64 | 1.20 ₅ | 0.15 | 1.40 ₅ | 21.48 |
| 1.17 | 0.76 | 1.30 | 0.18 | 1.59 | 22.22 |
| 1.23 | 0.88 | 1.40 | 0.20 ₅ | 1.80 | 22.96 |
| 1.27 | 1.00 | 1.50 | 0.23 | 2.00 | 26.67 |
| 1.33 | 1.08 | 1.60 ₅ | 0.25 | 2.19 | 35.55 ₅ |
| 1.37 | 1.20 | 1.70 | 0.27 | 2.39 | 54.81 |
| 1.43 | 1.28 | 1.80 ₅ | 0.30 | 2.58 | 85.92 ₅ |
| 1.47 | 1.32 | 1.91 | 0.32 | 2.78 | 115.55 ₅ |
| 1.53 | 1.40 | 2.01 | 0.35 | 2.99 | 142.22 |
| 1.58 | 1.48 | 2.11 | 0.38 ₅ | 3.17 ₅ | 171.85 |
| 1.63 | 1.52 | 2.18 | 0.41 | 3.38 | 201.48 |
| 1.67 | 1.56 | | | 3.58 | 232.59 |
| 1.73 | 1.64 | | | 3.78 | 266.67 |
| 1.78 | 1.68 | | | | |
| 1.83 | 1.72 | | | | |
| 1.87 | 1.80 | | | | |
| 1.92 | 1.88 | | | | |
| 1.98 | 1.96 | | | | |
| 2.02 | 2.04 | | | | |
| 2.07 | 2.16 | | | | |
| 2.11 | 2.24 | | | | |
| 2.15 | 2.36 | | | | |
| 2.18 | 2.52 | | | | |
| 2.22 | 2.68 | | | | |
| 2.29 | 2.96 | | | | |
| 2.32 | 3.20 | | | | |

Table 16 Tabulated numerical datapoints collated from Cahalane et al. [35]

| λ [–] | P [kPa] |
|-------------------|-----------|
| 0.20 ₅ | – 37.33 |
| 0.26 ₅ | – 21.78 |
| 0.35 | – 11.56 |
| 0.45 | – 4.57 |
| 0.58 | – 1.85 |
| 0.69 | – 0.86 |
| 1.00 | 0 |
| 1.10 | 0.93 |
| 1.22 | 2.00 |
| 1.30 | 2.67 |
| 1.40 | 3.33 |
| 1.53 ₅ | 4.44 |
| 1.70 | 5.56 |

Table 17 Tabulated numerical datapoints collated from Sugerman et al. [36]

| γ [–] | T_{ss} [kPa] | P_{22} [kPa] |
|---------------------|---------------------|-------------------|
| – 0.5 | – 0.92 | 0.33 ₅ |
| – 0.45 | – 0.60 | 0.21 ₅ |
| – 0.40 | – 0.38 ₅ | 0.14 |
| – 0.30 ₅ | – 0.18 | 0.06 |
| – 0.25 | – 0.11 | 0.03 |
| – 0.20 | – 0.05 | 0.01 ₅ |
| – 0.16 | – 0.04 | 0.01 |
| – 0.11 | – 0.01 | 0.00 ₂ |
| 0 | 0 | 0 |
| 0.09 | 0.01 | 0.00 ₂ |
| 0.16 | 0.04 | 0.01 |
| 0.20 | 0.06 | 0.02 |
| 0.25 | 0.12 | 0.04 ₅ |
| 0.30 ₅ | 0.22 | 0.07 ₅ |
| 0.39 | 0.49 | 0.16 |
| 0.45 | 0.74 | 0.24 |
| 0.5 | 1.09 | 0.36 |

References

1. Treloar, L.R.G.: The elasticity of a network of long-chain molecules - II. *Trans. Faraday Soc.* **39**, 241–246 (1943). <https://doi.org/10.1039/TF9433900241>
2. Mooney, M.: A theory of large elastic deformation. *J. Appl. Phys.* **11**, 582–592 (1940). <https://doi.org/10.1063/1.1712836>
3. Rivlin, R.S.: Large elastic deformations of isotropic materials IV. Further developments of the general theory. *Philos. Trans. R. Soc. Lond. A* **241**, 379–397 (1948). <https://doi.org/10.1098/rsta.1948.0024>
4. Destrade, M., Saccomandi, G., Sgura, I.: Methodical fitting for mathematical models of rubber-like materials. *Proc. R. Soc. A* **473**, 20160811 (2017). <https://doi.org/10.1098/rspa.2016.0811>
5. Ricker, A., Wriggers, P.: Systematic fitting and comparison of hyperelastic continuum models for elastomers. *Arch. Comput. Methods Eng.* **30**, 2257–2288 (2023). <https://doi.org/10.1007/s11831-022-09865-x>
6. Marckmann, G., Verron, E.: Comparison of hyperelastic models for rubber-like materials. *Rubber Chem. Technol.* **79**, 835–858 (2006). <https://doi.org/10.5254/1.3547969>
7. Steinmann, P., Hossain, M., Possart, G.: Hyperelastic models for rubber-like materials: consistent tangent operators and suitability for Treloar’s data. *Arch. Appl. Mech.* **82**, 1183–1217 (2012). <https://doi.org/10.1007/s00419-012-0610-z>
8. Hossain, M., Steinmann, P.: More hyperelastic models for rubber-like materials: consistent tangent operators and comparative study. *J. Mech. Behav. Mater.* **22**, 27–50 (2013). <https://doi.org/10.1515/jmbm-2012-0007>
9. Hossain, M., Amin, A.F.M.S., Kabir, M.N.: Eight-chain and full-network models and their modified versions for rubber hyperelasticity: a comparative study. *J. Mech. Behav. Mater.* **24**, 11–24 (2015). <https://doi.org/10.1515/jmbm-2015-0002>
10. Dal, H., Açıkgöz, K., Badienia, Y.: On the performance of isotropic hyperelastic constitutive models for rubber-like materials: a state of the art review. *Appl. Mech. Rev.* **73**, 020802 (2021). <https://doi.org/10.1115/1.4050978>
11. He, H., Zhang, Q., Zhang, Y., Chen, J., Zhang, L., Li, F.: A comparative study of 85 hyperelastic constitutive models for both unfilled rubber and highly filled rubber nanocomposite material. *Nano Mater. Sci.* **4**, 64–82 (2022). <https://doi.org/10.1016/j.nanoms.2021.07.003>

12. Anssari-Benam, A., Bucchi, A., Horgan, C.O., Saccomandi, G.: Assessment of a new isotropic hyperelastic constitutive model for a range of rubber-like materials and deformations. *Rubber Chem. Technol.* **95**, 200–217 (2022). <https://doi.org/10.5254/rct.21.78975>
13. Anssari-Benam, A., Horgan, C.O.: A three-parameter structurally motivated robust constitutive model for isotropic incompressible unfilled and filled rubber-like materials. *Eur. J. Mech. A Solids* **95**, 104605 (2022). <https://doi.org/10.1016/j.euromechsol.2022.104605>
14. Anssari-Benam, A., Destrade, M., Saccomandi, G.: Modelling brain tissue elasticity with the Ogden model and an alternative family of constitutive models. *Philos. Trans. R. Soc. A* **380**, 20210325 (2022). <https://doi.org/10.1098/rsta.2021.0325>
15. Anssari-Benam, A.: Large isotropic elastic deformations: on a *comprehensive* model to correlate the theory and experiments for incompressible rubber-like materials. *J. Elast.* **153**, 219–244 (2023). <https://doi.org/10.1007/s10659-022-09982-5>
16. Anssari-Benam, A.: Comparative modelling results between a separable and a non-separable form of principal stretches-based strain energy functions for a variety of isotropic incompressible soft solids: Ogden model compared with a *parent* model. *Mech. Soft Mater.* **5**, 2 (2023). <https://doi.org/10.1007/s42558-023-00050-z>
17. Anssari-Benam, A.: On a new class of non-Gaussian molecular based constitutive models with limiting chain extensibility for incompressible rubber-like materials. *Math. Mech. Solids* **26**, 1660–1674 (2021). <https://doi.org/10.1177/10812865211001094>
18. Anssari-Benam, A., Bucchi, A., Saccomandi, G.: On the central role of the invariant in nonlinear elasticity. *Int. J. Eng. Sci.* **163**, 103486 (2021). <https://doi.org/10.1016/j.ijengsci.2021.103486>
19. Ogden, R.W., Saccomandi, G., Sgura, I.: Fitting hyperelastic models to experimental data. *Comput. Mech.* **34**, 484–502 (2004). <https://doi.org/10.1007/s00466-004-0593-y>
20. Treloar, L.R.G.: Stress-strain data for vulcanised rubber under various types of deformation. *Trans. Faraday Soc.* **40**, 59–70 (1944). <https://doi.org/10.1039/TF9444000059>
21. Kawabata, S., Matsuda, M., Tei, K., Kawai, H.: Experimental survey of the strain energy density function of isoprene rubber vulcanizate. *Macromolecules* **14**, 154–162 (1981). <https://doi.org/10.1021/ma50002a032>
22. Lahellec, N., Mazerolle, F., Michel, J.C.: Second-order estimate of the macroscopic behavior of periodic hyperelastic composites: theory and experimental validation. *J. Mech. Phys. Solids* **52**, 27–49 (2004). [https://doi.org/10.1016/S0022-5096\(03\)00104-2](https://doi.org/10.1016/S0022-5096(03)00104-2)
23. Hohenberger, T.W., Windslow, R.J., Pugno, N.M., Busfield, J.J.C.: A constitutive model for both low and high strain nonlinearities in highly filled elastomers and implementation with user-defined material subroutines in ABAQUS. *Rubber Chem. Technol.* **92**, 653–686 (2019). <https://doi.org/10.5254/rct.19.80387>
24. Meunier, L., Chagnon, G., Favier, D., Orgeas, L., Vacher, P.: Mechanical experimental characterisation and numerical modelling of an unfilled silicone rubber. *Polym. Test.* **27**, 765–777 (2008). <https://doi.org/10.1016/j.polymertesting.2008.05.011>
25. Jiang, M., Dai, J., Dong, G., Wang, Z.: A comparative study of invariant-based hyperelastic models for silicone elastomers under biaxial deformation with the virtual fields method. *J. Mech. Behav. Biomed. Mater.* **136**, 105522 (2022). <https://doi.org/10.1016/j.jmbbm.2022.105522>
26. Yohsuke, B., Urayama, K., Takigawa, T., Ito, K.: Biaxial strain testing of extremely soft polymer gels. *Soft Matter* **7**, 2632–2638 (2011). <https://doi.org/10.1039/C0SM00955E>
27. Mai, T.-T., Matsuda, T., Nakajima, T., Gong, J.P., Urayama, K.: Distinctive characteristics of internal fracture in tough double network hydrogels revealed by various modes of stretching. *Macromolecules* **51**, 5245–5257 (2018). <https://doi.org/10.1021/acs.macromol.8b01033>
28. Saadedine, M., Zaïri, F., Ouali, N., Mesbah, A.: A micromechanics-based model for visco-super-elastic hydrogel-based nanocomposites. *Int. J. Plast.* **144**, 103042 (2021). <https://doi.org/10.1016/j.ijplas.2021.103042>
29. Mihai, L.A., Mistry, D., Raistrick, T., Gleeson, H.F., Goriely, A.: A mathematical model for the auxetic response of liquid crystal elastomers. *Phil. Trans. R. Soc. A* **380**, 20210326 (2022). <https://doi.org/10.1098/rsta.2021.0326>
30. Raistrick, T., Zhang, Z., Mistry, D., Mattsson, J., Gleeson, H.F.: Understanding the physics of the auxetic response in a liquid crystal elastomer. *Phys. Rev. Res.* **3**, 023191 (2021). <https://doi.org/10.1103/PhysRevResearch.3.023191>
31. Tokumoto, H., Zhou, H., Takebe, A., Kamitani, K., Kojio, K., Takahara, A., Bhattacharya, K., Urayama, K.: Probing the in-plane liquid-like behavior of liquid crystal elastomers. *Sci. Adv.* **7**, eabe9495 (2021). <https://doi.org/10.1126/sciadv.abe9495>
32. Merkel, D.R., Saha, R.K., Yakacki, C.M., Frick, C.P.: Mechanical energy dissipation in polydomain nematic liquid crystal elastomers in response to oscillating loading. *Polymer* **166**, 148–154 (2019). <https://doi.org/10.1016/j.polymer.2019.01.042>
33. Mihai, L.A., Goriely, A.: A pseudo-anelastic model for stress softening in liquid crystal elastomers. *Proc. R. Soc. A* **476**, 20200558 (2020). <https://doi.org/10.1098/rspa.2020.0558>
34. Budday, S., Sommer, G., Birkl, C., Langkammer, C., Haybaeck, J., Kohnert, J., Bauer, M., Paulsen, F., Steinmann, P., Kuhl, E., Holzapfel, G.A.: Mechanical characterization of human brain tissue. *Acta Biomater.* **48**, 319–340 (2017). <https://doi.org/10.1016/j.actbio.2016.10.036>
35. Cahalane, R.M.E., de Vries, J.J., de Maat, M.P.M., van Gaalen, K., van Beusekom, H.M., van der Lugt, A., Fereidoonzhad, B., Akyildiz, A.C., Gijsen, F.J.H.: Tensile and compressive mechanical behaviour of human blood clot analogues. *Ann. Biomed. Eng.* (2023). <https://doi.org/10.1007/s10439-023-03181-6>
36. Sugeran, G.P., Kakaletsis, S., Thakkar, P., Chokshi, A., Parekh, S.H., Rausch, M.K.: A whole blood thrombus mimic: constitutive behavior under simple shear. *J. Mech. Behav. Biomed. Mat.* **115**, 104216 (2021). <https://doi.org/10.1016/j.jmbbm.2020.104216>
37. Gent, A.N.: A new constitutive relation for rubber. *Rubber Chem. Technol.* **69**, 59–61 (1996). <https://doi.org/10.5254/1.3538357>
38. Beatty, M.F.: Topics in finite elasticity: hyperelasticity of rubber, elastomers, and biological tissues - with examples. *Appl. Mech. Rev.* **40**, 1699–1734 (1987). <https://doi.org/10.1115/1.3149545>
39. Pucci, E., Saccomandi, G.: A note on the Gent model for rubber-like materials. *Rubber Chem. Technol.* **75**, 839–852 (2002). <https://doi.org/10.5254/1.3547687>

40. Puglisi, G., Saccomandi, G.: Multi-scale modelling of rubber-like materials and soft tissues: an appraisal. *Proc. R. Soc. A* **472**, 20160060 (2016). <https://doi.org/10.1098/rspa.2016.0060>
41. Horgan, C.O., Saccomandi, G.: Simple torsion of isotropic, hyperelastic, incompressible materials with limiting chain extensibility. *J. Elast.* **56**, 159–170 (1999). <https://doi.org/10.1023/A:1007606909163>
42. Saccomandi, G.: Universal results in finite elasticity. In: Fu, Y.B., Ogden, R.W. (eds.) *Nonlinear Elasticity: Theory and Applications*, pp. 97–134. Cambridge University Press, Cambridge (2001). <https://doi.org/10.1017/CBO9780511526466.004>
43. Wineman, A.: Some results for generalized neo-Hookean elastic materials. *Int. J. Non-Linear Mech.* **40**, 271–279 (2005). <https://doi.org/10.1016/j.ijnonlinmec.2004.05.007>
44. Carroll, M.M.: A strain energy function for vulcanized rubbers. *J. Elast.* **103**, 173–187 (2011). <https://doi.org/10.1007/s10659-010-9279-0>
45. Mihai, L.A., Goriely, A.: Positive or negative Poynting effect? The role of adscititious inequalities in hyperelastic materials. *Proc. R. Soc. A* **467**, 3633–3646 (2011). <https://doi.org/10.1098/rspa.2011.0281>
46. Yeoh, O.H.: Characterisation of elastic properties of carbon-black-filled rubber vulcanizates. *Rubber Chem. Technol.* **63**, 792–805 (1990). <https://doi.org/10.5254/1.3538289>
47. Nunes, L.C.S.: Mechanical characterization of hyperelastic polydimethylsiloxane by simple shear test. *Mater. Sci. Eng. A* **528**, 1799–1804 (2011). <https://doi.org/10.1016/j.msea.2010.11.025>
48. Lopez-Pamies, O.: A new II-based hyperelastic model for rubber elastic materials. *C. R. Mecanique* **338**, 3–11 (2010). <https://doi.org/10.1016/j.crme.2009.12.007>
49. Anssari-Benam, A., Bucchi, A.: Modelling the deformation of the elastin network in the aortic valve. *J. Biomech. Eng.* **140**, 011004 (2018). <https://doi.org/10.1115/1.4037916>
50. Anssari-Benam, A., Bucchi, A.: A generalised neo-Hookean strain energy function for application to the finite deformation of elastomers. *Int. J. Non-Linear Mech.* **128**, 103626 (2021). <https://doi.org/10.1016/j.ijnonlinmec.2020.103626>
51. Anssari-Benam, A., Bucchi, A., Destrade, M., Saccomandi, G.: The generalised mooney space for modelling the response of rubber-like materials. *J. Elast.* **151**, 127–141 (2022). <https://doi.org/10.1007/s10659-022-09889-1>
52. Payne, A.R., Whittaker, R.E.: Low strain dynamic properties of filled rubbers. *Rubber Chem. Technol.* **44**, 440–478 (1971). <https://doi.org/10.5254/1.3547375>
53. Anssari-Benam, A., Horgan, C.O.: On modelling simple shear for isotropic incompressible rubber-like materials. *J. Elast.* **147**, 83–111 (2021). <https://doi.org/10.1007/s10659-021-09869-x>
54. Choi, H.S., Vito, R.P.: Two-dimensional stress-strain relationship for canine pericardium. *J. Biomech. Eng.* **112**, 153–159 (1990). <https://doi.org/10.1115/1.2891166>
55. Brossollet, L.J., Vito, R.P.: A new approach to mechanical testing and modeling of biological tissues, with application to blood vessels. *J. Biomech. Eng.* **118**, 433–439 (1996). <https://doi.org/10.1115/1.2796028>
56. Park, S., Oh, Y., Moon, J., Chung, H.: Recent trends in continuum modeling of liquid crystal networks: a mini-review. *Polymers* **15**, 1904 (2023). <https://doi.org/10.3390/polym15081904>
57. Holzapfel, G.A., Ogden, R.W.: On planar biaxial tests for anisotropic nonlinearly elastic solids: a continuum mechanical framework. *Math. Mech. Solids* **14**, 474–489 (2009). <https://doi.org/10.1177/1081286507084411>
58. Ogden, R.W.: *Non-linear Elastic Deformations*. Dover Publications Inc, New York (1997)
59. Gent, A.N., Thomas, A.G.: Forms for the stored (strain) energy function for vulcanized rubber. *J. Polym. Sci.* **28**, 625–628 (1958). <https://doi.org/10.1002/pol.1958.1202811814>
60. Arruda, E.M., Boyce, M.C.: A three-dimensional constitutive model for the large stretch behavior of rubber elastic materials. *J. Mech. Phys. Solids* **41**, 389–412 (1993). [https://doi.org/10.1016/0022-5096\(93\)90013-6](https://doi.org/10.1016/0022-5096(93)90013-6)